Particle Acceleration at Relativistic Shock Fronts[1]

John G. Kirk

Max-Planck-Institut für Physik und Astrophysik

Institut für Astrophysik

Garching bei München

[1]Thesis submitted in partial fulfilment of the conditions for admission to the degree of Dr. rer. nat. habil. in the Ludwig-Maximillians-Universität, München, January 1988.

Abstract

A theory of particle acceleration is presented which is based on the first-order Fermi Process occurring in the converging fluid flow close to a shock front. In contrast to the standard diffusive theory of particle acceleration at shock fronts [22], this theory permits one to treat particles whose velocity is not necessarily large compared to that of the fluid through the shock. As such, it finds application in two physical situations: i) the acceleration of low-energy ions at nonrelativistic (e.g. interplanetary) shocks and ii) the acceleration of particles at relativistic shocks (e.g. in quasars and active galactic nuclei). This thesis emphasizes the latter application.

The pitch-angle distribution of accelerated particles is intrinsically anisotropic, in the theory developed here, and depends on the nature of the pitch-angle scattering processes assumed to occur in the background fluid. The quasi-linear theory of plasma physics predicts one model of the scattering which corresponds to diffusion in pitch-angle. However, this model cannot represent the processes occurring in a plasma with an appreciable level of turbulence. Therefore, a semi-empirical model is also investigated, which permits large-angle scattering events as well as pitch-angle diffusion. At the present stage of development of the theory, it is possible to draw only tentative conclusions about the effects of strong turbulence by employing this kind of approach.

A detailed description of the method used in solving for the anisotropic pitch-angle distribution is presented, followed by the results obtained upon applying it to various kinds of relativistic shock fronts. The hydrodynamics of

such shocks has not been investigated in sufficient depth in the literature to permit realistic jump conditions to be extracted, so that a chapter of the thesis is devoted to this topic. For each kind of shock, the index of the power-law spectrum of accelerated particles is given. Since this depends on the pitch-angle scattering operator, the results are presented separately for different assumptions concerning the turbulence. In addition, the effects of the large-angle scattering operator are discussed, and seen to have a significant, but not dramatic effect.

Finally, a short discussion of the application to the problem of particle acceleration in the relativistic outflows associated with quasars and active galactic nuclei is given. There seems to be no intrinsic difficulty in producing the type of particle distribution which is implied by the observations. In principle, the theory is capable of enhancing the predictive power of models of these objects which, at present, postulate the injection of the necessary energetic particles.

A preliminary and somewhat less general account of this theory is presented in [49], and an application to interplanetary shock fronts is discussed in [47]. The effects of the large-angle operator are investigated in [50].

Contents

CHAPTER I

Introduction

Particle acceleration is a process which seems to occur in Nature under a wide variety of circumstances. Direct observations of accelerated particles themselves are made in the case of cosmic rays arriving at Earth, as well as in the case of energetic particles found in the Earth's ionosphere, magnetosphere and in interplanetary space. Apart from this, the electromagnetic radiation emitted by accelerated electrons or positrons is detected from sources ranging from the magnetosphere (terrestrial kilometric radiation, for example) to the most distant objects in the universe — radio galaxies and quasars.

Many theories have been developed to account for particle acceleration in the various situations mentioned above, and these are extensively discussed in numerous conference proceedings, review articles and monographs. From a general point of view, the article by Parker [75] and the monographs by Melrose [68,69] form excellent introductions. The aim of this thesis is to present a detailed account of a theory of particle acceleration which applies in the vicinity of shock fronts moving at relativistic velocities, as well as in certain other situations.

About a decade ago, Fermi's ideas [27,28] concerning the acceleration of cosmic rays were revived by the discovery of a mechanism now called "diffusive acceleration at shock fronts" [4,6,53,10]. The most important modification to Fermi's proposal was that instead of assuming that cosmic rays are scat-

tered by large-scale inhomogeneities in the interstellar medium, it was noticed that scattering in the turbulent plasma to be found in the neighbourhood of shock fronts would be much more efficacious. Fermi had already realized [28] that *converging* scattering centres are much better at particle acceleration than are ones which move in random directions. The new idea of 1977/78 was the realization that scattering centres fixed in a fluid *always* converge at a shock front.

It is well-known from, for example, the theory of radiative transfer [17], that particles whose distribution function is kept close to isotropy by a scattering process behave as if they were diffusing in space. More precisely, the flux of such particles is linearly related to the gradient of their density by Fick's law — the constant of proportionality being the spatial diffusion coefficient. Diffusion in space implies that some particles repeatedly cross and recross the shock front, and are, therefore, systematically accelerated by the converging scattering centres. Combined with a finite probability for escape from the shock front into the downstream fluid, this acceleration mechanism yields a distribution function which is a power-law in momentum under a wide variety of physical conditions [22,3,30,7]. The original papers and much subsequent work on diffusive acceleration has been motivated by the problem of the acceleration of cosmic rays. However, the mechanism is so general that many other applications are possible. Almost any location in which kinetic energy is thermalized by a shock front is likely to be a suitable site for the acceleration of charged particles — both ions and electrons. The latter, of course, may be expected to radiate profusely, which has led to the suggested identification of nonthermal radio sources with regions containing electrons accelerated at shock fronts. Additional support for this hypothesis is provided

by the slope of the observed spectrum of radio waves, which seems to arise from a power-law distribution of electrons. Even in objects as diverse as supernova remnants and the jets of radio galaxies, the spectral index required of the electron distribution is not too different from that of cosmic rays [89].

One attractive application of particle acceleration models concerns quasars and active galactic nuclei (AGN's). The difficulties posed by the apparently extremely high luminosity of these objects are well-known (see articles in [95]). Indeed, they have provoked controversy and appeals for the necessity of "new physics" [2] more often than any other astrophysical phenomenon. Even a qualitative understanding of how those particles which radiate could have been accelerated is, therefore, of considerable interest. Because of this sense of urgency, the theory of diffusive acceleration at shock fronts has been applied [42,94]. However, the basic assumption of the theory is almost certainly violated in the physical conditions pertaining in these objects. Rapid variability, high brightness temperatures in the radio regime and observed superluminal motion form the observational support for the model originally devised by Rees [83] which requires relativistic motion of the radiating particles towards the observer, probably in the form of directed motion along a "jet" [8,5]. If fluid flows at relativistic bulk speed with respect to its surroundings, thermalization of its kinetic energy seems unlikely to occur by means of a shock front through which the flow is nonrelativistic. However, only if this possibility is realized in practice, is it possible for pitch-angle scattering to maintain an almost isotropic distribution of accelerated particles. For relativistic shocks, on the other hand, there can exist no distribution which is almost isotropic in both the frame of the upstream fluid and the frame of the downstream fluid. The application to quasars and AGN's, therefore, requires the development of

a new theory of particle acceleration at shock fronts: one in which the motion of the particles is not assumed to be diffusive in space.

Until recently, little work had been done on the problem of acceleration at relativistic shocks. Considering the microphysics, Peacock [78] investigated two conjectures which he advanced about the angular distribution of accelerated particles. But discussions of the hydrodynamics of the gas of accelerated particles seemed to imply that special conditions are required for acceleration to occur at all at relativistic shocks [103,104]. In addition to this, there was a widely held belief that relativistic shocks are unable to accelerate particles efficiently (see, for example [7], page 34).

The difficulties involved in constructing a theory of acceleration at relativistic shocks, which is analogous to the theory of diffusive acceleration, are considerable. The basic process by which particles gain energy remains the same — namely by scattering between converging fluid elements upstream and downstream of a shock front. However, abandoning the diffusion approximation introduces an additional degree of freedom — the angular distribution. As in the theory of radiative transfer, the complexity of the problem is thereby increased dramatically, necessitating the use of more powerful methods of solution. In fact, particle acceleration poses an even more daunting problem, because the nature of the basic interactions determining the transport process (photon scattering in the case of radiative transfer) is largely unknown. In the theory of diffusive acceleration, the details of the process responsible for isotropizing the particle distribution are unimportant. However, once one takes the step of dropping the diffusion approximation, it becomes essential to model the pitch-angle scattering operator.

Not only the environment of relativistic shocks demands an approach

divorced from the diffusion approximation, but also any situation in which particles with a speed comparable to that of the fluid are accelerated. Low energy, heavy ions at interplanetary shocks fall into this category [47], as do all particles initially, if they are to be accelerated at a shock front and are assumed to be injected from the thermal plasma of the background. It is here that there is hope of observational help in attacking the problem of modelling the pitch-angle scattering operator. Because the acceleration of low energy ions depends on this operator, it may be possible to use *in situ* observations of the angular distribution to constrain the models. One other source of assistance lies in computer simulations of charged particle transport and of the formation of parallel shocks [107,82]. Some of these suggest that strong plasma turbulence may introduce a qualitatively different kind of scattering operator to that derived analytically for weak turbulence (i.e. in the quasi-linear theory).

This thesis presents a theory of particle acceleration at relativistic shock fronts, motivated by the application to shock fronts in relativistic outflows associated with quasars and AGN's. Because of the uncertainty involved with modelling the details of the plasma physics, the following approach is adopted. In the main investigation, the analytic results of quasi-linear theory are used, parameterized to allow for variations in the properties of the background turbulence, in order to permit a systematic parameter survey covering a wide range of different types of relativistic shock front. In addition, the possible effects of a large-angle scattering operator are discussed, using a particular shock front as an example. Such a scattering operator produces effects similar to those seen in the numerical simulations mentioned above and has recently been proposed as a semi-empirical method of accounting for the effects of strong turbulence [50]. Its inclusion in this thesis is intended to indicate the

extent to which the results of using a quasi-linear type of operator are likely to be changed in the presence of strong turbulence.

As a preliminary, the mathematical formulation of the transport equation is presented in §II, together with a description of the models used both for the quasi-linear type of scattering operator and for the large-angle scattering operator. This transport equation is to be used to solve the problem of test particle acceleration at parallel shocks propagating in a homogeneous background plasma. Of course, these conditions are somewhat idealized, but the first-order Fermi process appears to be most effective at a shock front whose normal is almost parallel to the plasma flow in both the upstream and downstream regions ("quasi-parallel" shocks), at least in interplanetary space [7]. Furthermore, homogeneity is required only on the relatively small length scale associated with the mean free path of an energetic particle. The test particle approximation is more drastic. Essentially, it consists of assuming that the particles under consideration do not contribute appreciably to the pressure in the fluid. The theory of diffusive shock acceleration has already proceeded far beyond this stage, but, in view of the greater complexity of the present theory, the assumption must still be retained. For consistency, it is necessary to assume that if particle distributions are produced with a power-law index s (see §4.3) less than 4, there exists a cut-off at high particle momenta, above which some saturation mechanism (such as discussed in [94]) prevents acceleration. In the absence of a cut-off, the pressure exerted by such a test particle distribution would diverge.

Although relativistic shocks are considered in several papers to be found in the literature, none of these presents the jump conditions to be expected for a gas with a plausible equation of state. Taub [97] discusses the

Rankine-Hugoniot equations which determine the jump conditions, but does not specify an equation of state for the fluid. Blandford and McKee [9] restrict their considerations to the limit of an ultrarelativistic gas and Königl [52] uses an approximation in which the adiabatic index of the gas (see equation 3.12) is assumed constant, although this is not in general true. The case in which the plasma returns to a state of complete thermodynamic equilibrium after passing through the shock front has been dealt with by Peacock [78], as well as another variation in which particles conserve their energy on crossing the shock. However, it seems to be more physically realistic to make a somewhat different assumption, namely that the kinetic energy of the upstream fluid is distributed amongst either only the ions, or only the electrons. The equation of state and the jump conditions across a strong shock are derived in §III under these assumptions. In addition, since it is quite likely that electron–positron pairs may be produced in large numbers in shocks close to the central engines of quasars [94], the possibility of the injection of a number of pairs at the shock front has been taken into account in computing the jump conditions.

The method of solving the transport equation is described in §IV. This chapter forms the heart of the thesis. The method has been described previously in a shorter and less general form [49] and has been applied to shocks in the interplanetary medium [47]. Although similar to the P_N method familiar from the theory of radiative transfer, it is significantly different, in that the distribution function is represented not as a sum of Legendre polynomials, but as a sum of eigenfunctions chosen to be particularly suitable to either the upstream or the downstream regions.

The application to relativistic shocks is presented in §V, and results in a single value of s, the power-law index of accelerated particles for each of

the shocks considered. Not only is a parameter survey presented, but also an attempt is made to indicate the effects of large-angle scattering on the results. If one assumes that electrons are the particles which are accelerated, then the value of s is, in principle, observable, since it is related to the spectrum of synchrotron radiation emitted [68]. In practice, the observed synchrotron radiation stems from the entire source, consisting not only of the shock front, but also of the downstream region in which the electrons cool. The size of this region depends on the frequency at which observations are made. Electrons which emit high frequency synchrotron radiation cool more quickly and fill a smaller volume than electrons which emit lower frequency radiation. Therefore, the complicating effects of large-scale inhomogeneities of the flow pattern are more prominent at lower frequencies, whereas the "cleanest" picture of the acceleration process is obtained at high frequencies. In §V, it is indicated how the results fit into a current model aimed at explaining the flaring behaviour of some quasars in the infra-red to microwave region of the spectrum [65]. Although much work remains to be done on detailed applications of the type indicated, the preliminary results are encouraging. Relativistic shocks are capable of accelerating particles by the first-order Fermi mechanism, and produce a power-law spectrum with an index which is close to that required by models of the emission regions of at least some quasars and AGN's. The uncertainty which results from lack of understanding of the scattering mechanisms present in strongly turbulent plasmas appears to have only a minor effect on these results.

CHAPTER II

The Transport Equation

The purpose of this chapter is to derive the transport equation which governs the propagation of energetic charged particles under certain simple conditions. Since the scope of this work is restricted to parallel shocks in an infinite homogenous medium, the only permitted spatial dependence is on the coordinate of the normal to the shock z. The fluid velocity upstream and downstream of the shock front, which is positioned at $z = 0$, are taken to be constants, and only stationary solutions of the problem are considered. The key point in the treatment is the use of *comoving coordinates* for the description of the particles, whilst retaining the coordinates of the shock frame for the spatial dependence. This technique is well-known in the theory of radiative transfer [16,70,86]. Under these conditions, one arrives at a relatively simple transport equation (2.26).

It is the processes which disturb or scatter particle trajectories which are ultimately responsible for Fermi acceleration, and these appear in the collision operator C. An explicit form for this operator is given in the quasi-linear theory of plasma physics, supplemented by some assumptions about the nature of the dominant MHD waves in the plasma, and their spectrum. This form is presented and its range of applicability briefly discussed. Several problems are known to occur when such a collision operator is adopted, for example there is very little scattering of particles with a pitch-angle close to 90°. Further-

more, it seems that the assumption of weak turbulence is violated even in the application to the relatively slow shocks of the interplanetary medium. The exact form of the collision operator given by the quasi-linear theory should, therefore, be considered more as an indication of how to model the interaction with turbulence, than as an exact representation of the scattering. The additional freedom gained by such a liberal interpretation can be used to remove the difficulties associated with scattering through 90°, introducing at the same time an adjustable parameter.

In the same vein, it is possible to generalize the quasi-linear operator (which contains essentially only pitch-angle diffusion) to include processes such as large-angle scattering. The motivation for such a course of action arises from the results of computer simulations of the propagation of charged particles in strongly turbulent plasmas [107]. The pitch-angle diffusion operator appears to be an adequate description of the particle transport only for levels of turbulence $\delta B/B < 1/10$. At higher levels of turbulence, particle trajectories are observed occasionally to undergo rapid changes of pitch-angle in a short time (a few gyro-periods) — behaviour not consistent with pitch-angle diffusion. Similar events have also been observed in simulations of the formation of parallel shocks [82], although in this case the particles involved were of only moderate energy. Occasional events of this type could have a marked effect on the acceleration process at relativistic shocks. However, a large measure of freedom is available in attempting to model the process, so that it is to be hoped that a detailed analysis of the simulations will be able to offer the constraints necessary for a realistic model in the near future. As this is beyond the scope of this thesis, only the simplest of possibilities is discussed, although the means by which more sophisticated models could be investigated are indicated briefly.

2.1 The Liouville Operator

The derivation starts with the unperturbed paths of charged particles in phase-space:

$$\begin{aligned} \frac{dx^a}{d\tau} &= p^a \\ \frac{dp^a}{d\tau} &= \frac{e}{m} F^a_b p^b - \Gamma^a_{bc} p^b p^c \end{aligned} \tag{2.1}$$

where x^a and p^a are the position and momentum four-vectors (latin indices run from 0 to 3), τ is the proper time, F^a_b is the field-strength tensor of the electromagnetic field, and Γ^a_{bc} is a connection coefficient. The equation refers to a particle of mass $m = \sqrt{p^a p_a}$ and charge e, units are adopted in which the speed of light is unity and the summation convention of Einstein is used. In the absence of collisions, that is when equation (2.1) describes the motion of the particle exactly, one arrives at the Liouville equation for the Lorentz invariant phase-space density F_0 of the particles [60,25]:

$$\frac{dx^a}{d\tau}\frac{\partial F_0}{\partial x^a} + \frac{dp^\lambda}{d\tau}\frac{\partial F_0}{\partial p^\lambda} = 0, \tag{2.2}$$

where the index λ is used in the second term because there are only three independent components of p^a for a particle of fixed mass and greek indices are taken to run from 1 to 3.

Collisions may be accounted for by replacing the right-hand side of (2.2) by $(\partial F_0/\partial\tau)_{\text{collisions}}$; sources and sinks of particles may be incorporated in a similar manner. These terms are usually evaluated in a particular frame. In the case of radiative transfer, this would be the frame of the fluid containing the scattering centres and the absorbing or emitting atoms. For charged particles, the scattering arises from MHD waves, and is normally calculated in the frame in which the fluid supporting such waves is locally at rest, although other

frames have been considered [91]. On the other hand, the solutions of interest are those which are stationary in the frame in which the shock front is at rest. It is, therefore, desirable to mix the reference systems used in the Liouville operator, expressing the position x^a in the shock frame, whilst measuring the momentum p^a in the local fluid frame. Introducing the notation $\hat{}$ for quantities measured in the local fluid frame (quantities without a circumflex are measured in the shock frame) and the Lorentz boost L^a_b from the shock frame to the local fluid frame, one obtains the equation [86]

$$\hat{L}^a_b \hat{p}^b \frac{\partial F_0}{\partial x^a} - \hat{\Gamma}^\lambda_{bc} \hat{p}^b \hat{p}^c \frac{\partial F_0}{\partial \hat{p}^\lambda} + \frac{e}{m} \hat{F}^\lambda_b \hat{p}^b \frac{\partial F_0}{\partial \hat{p}^\lambda} = \hat{p}^0 (\hat{C}(F_0) + \hat{S}), \tag{2.3}$$

in which the collision operator $\hat{C}$ and the source term $\hat{S}$ as measured in the fluid frame have been introduced. In the case at hand, the velocity four-vector of the fluid flow is constant $U^a = (\Gamma, 0, 0, \Gamma u)$, where $\Gamma = (1-u^2)^{-1/2}$ and the magnetic field B_0 is in the z–direction and also constant. Thus, provided the shock frame is an inertial frame (as will be assumed), the fluid frame is also inertial, and the connection coefficients vanish. Then, a straightforward calculation leads to the transport equation

$$\begin{aligned} &\Gamma(1 + u\hat{v}\hat{\mu}) \frac{\partial F_0}{\partial t} + \Gamma(u + \hat{v}\hat{\mu}) \frac{\partial F_0}{\partial z} \\ &+ \hat{p}_x \frac{\partial F_0}{\partial x} + \hat{p}_y \frac{\partial F_0}{\partial y} + \frac{e}{m} B_0 \left(\hat{v}_y \frac{\partial F_0}{\partial \hat{p}_x} - \hat{v}_x \frac{\partial F_0}{\partial \hat{p}_y} \right) = \hat{C}(F_0) + \hat{S}. \end{aligned} \tag{2.4}$$

In this equation we have introduced the particle velocity $\hat{v} = \hat{p}/\hat{p}^0$ (where $\hat{p} = (\hat{p}^\alpha \hat{p}_\alpha)^{1/2}$) and the cosine of the pitch-angle $\hat{\mu} = \hat{p}_z/\hat{p}$, and have used the notation $\hat{p}_{x,y,z}$ and $\hat{v}_{x,y,z}$ for the components of $\hat{p}^\alpha$ and $\hat{v}^\alpha$. In problems concerning the transport of charged particles, one is usually interested in only the average of the phase-space density over the gyro-phase of the particles:

$$f(z, t, \hat{p}, \hat{\mu}) = \frac{1}{2\pi} \int_0^{2\pi} d\hat{\phi}\, F_0(z, t, \hat{p}, \hat{\mu}, \hat{\phi}). \tag{2.5}$$

Further simplifying the situation to distributions which depend only on the spatial coordinate z, as indicated in equation (2.5), gives

$$\Gamma(1+uv\mu)\frac{\partial f}{\partial t}+\Gamma(u+v\mu)\frac{\partial f}{\partial z} = C(f)+S(f), \tag{2.6}$$

in which, as in the remainder of this thesis, the circumflex notation for quantities in the fluid frame has been dropped.

2.2 The Collision Operator in the Quasi-Linear Theory

The diffusion coefficients for scattering off hydromagnetic waves have been given by [67]. The present investigation, however, will be restricted to the case in which only Alfvén waves propagating parallel and antiparallel to the magnetic field are considered. These are, in general, the waves with the smallest damping rates, and can be expected to dominate the turbulence far from the shock. [57,58,26]. Luhmann [61] has given the following expressions for the diffusion coefficients in this approximation, including the effects of a non-vanishing value of the Alfvén velocity v_A:

$$\begin{aligned} D_{\mu\mu} &= \left(\frac{2\pi Ze}{cp}\right)^2 \frac{v\mathcal{E}_B(k_\parallel^0)}{|\mu - v_A/v|}(1-\mu^2)(1-\mu v_A/v)^2 \\ D_{\mu p} &= D_{p\mu} = D_{\mu\mu}\frac{pv_A}{(v-\mu v_A)} \\ D_{pp} &= D_{\mu\mu}\left(\frac{pv_A}{(v-\mu v_A)}\right)^2 , \end{aligned} \tag{2.7}$$

where Ze is the charge of the ion, $\mathcal{E}_B(k_\parallel^0)$ is the spectral energy density of the turbulence and the resonant value of the wave number is $k_\parallel^0 = \Omega/|v_A - \mu v|$ with $\Omega = |ZeBv/cp|$ the gyro-frequency in the magnetic field B. Equation (2.7), which corrects some minor errors in Luhmann's expression [91], includes only forward propagating waves. The extension to waves propagating in each direction is straightforward (see, for example, [48]).

The diffusion coefficients $D_{\mu p}$ and D_{pp} are usually neglected in theories of first-order Fermi acceleration. For scattering off Alfvén waves, the ratio of $D_{\mu\mu}$ to $D_{\mu p}$ and D_{pp} is v/pv_A and $(v/pv_A)^2$ respectively. Compared to both v and u, v_A is small in the conditions envisaged, but the effect of the $D_{\mu p}$ and D_{pp} terms is, of course, qualitatively different to that of pitch-angle diffusion, since they produce a change in the particle momentum. Nevertheless, it is possible to make reasonable estimates of their effect. The term containing $D_{\mu p}$ vanishes if the distribution is isotropic, but, by estimating the anisotropy close to a shock to be $|\partial f/\partial\mu| < fu/v$, one finds a rate of change of momentum which is $|\Delta p/\Delta t| < D_{\mu p}u/v$. However, particles accelerated by the first-order Fermi process systematically gain momentum $\Delta p/p \approx u/v$ each time a cycle of crossing and recrossing the shock front is completed. This takes a time $\Delta t \approx v/uD_{\mu\mu}$, [22] and dominates the effect of the $D_{\mu p}$ term provided $v_A << u$. Similarly, second-order Fermi (or statistical) acceleration produced by the D_{pp} term is negligible provided $(v_A/u)^2 << u/v$. This condition is fulfilled for relativistic shocks unless the magnetic field is extremely strong — a situation which occurs in models of Fermi acceleration as applied to neutron stars [43]. However, for present purposes, it is sufficient to consider only the pitch-angle diffusion coefficient $D_{\mu\mu}$. Assuming that the energy density in forward and backward propagating waves of each polarization is equal, and can be modelled by a power-law one finds:

$$\mathcal{E}_B(k_\parallel) = \alpha_t \frac{v}{\Omega}\left(\frac{k_\parallel v}{\Omega}\right)^{-q} \tag{2.8}$$

where

$$\alpha_t = \frac{\pi\Omega}{2v}\frac{\mathcal{E}_B(\Omega/v)}{B^2/8\pi} \tag{2.9}$$

is a dimensionless normalization of the turbulence. The expression for the

pitch-angle diffusion coefficient then simplifies to

$$\begin{aligned} D_{\mu\mu} &= \alpha_t \Omega (1-\mu^2) \left[|\mu - v_A/v|^{q-1} + |\mu + v_A/v|^{q-1} \right] \\ &= \alpha_t \Omega \hat{D}_{\mu\mu} \end{aligned}$$

to lowest order in v_A. The dimensionless pitch-angle diffusion coefficient $\hat{D}_{\mu\mu}$ has also been introduced in this equation. The collision operator for pitch-angle diffusion can then be written

$$\left(\frac{\partial f}{\partial t} \right)_{\text{collisions}} = \nu_s C_s f, \tag{2.10}$$

where

$$\nu_s = \alpha_t \Omega$$

and

$$C_s = \frac{\partial}{\partial \mu} \hat{D}_{\mu\mu} \frac{\partial}{\partial \mu}. \tag{2.11}$$

The function $\hat{D}_{\mu\mu}$ is displayed in Figure 2.1 for $q = 2$ and $v_A/v = 1/50$. There is a prominent dip around $\mu = 0$, where $\hat{D}_{\mu\mu}$ is a factor of about $(v_A/v)^{q-1}$ below its maximum. It is at these values of the pitch-angle at which particles resonate with Alfvén waves of very short wavelength. A power-law spectrum such as that of equation (2.8), implies very little scattering at such points. In addition, short wavelength Alfvén waves suffer damping by thermal ions, which has led to the suggestion that particles with $\mu \approx 0$ undergo no scattering at all [34]. A detailed investigation of this effect by Davilla [21] has shown that this may be the case for particles which are not highly relativistic. However, several investigations of the higher order nonlinear effects of the waves on the particle orbits [101,38,32] indicate that, in fact, a substantial amount of pitch-angle scattering is present at small μ. Thus, although $\hat{D}_{\mu\mu}$ does not go to zero for finite v_A [26], it is nevertheless desirable to incorporate the findings of

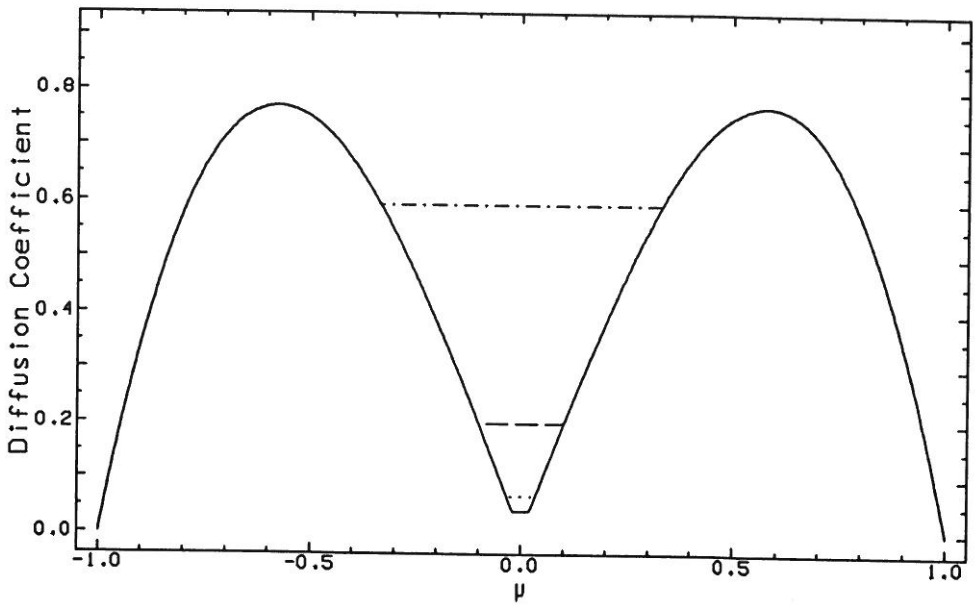

Figure 2.1: The pitch-angle diffusion coefficient as a function of the cosine μ of the pitch-angle, according to the quasi-linear theory. Alfvén turbulence with a spectrum $q = 2$ is assumed, and the "hole" around $\mu = 0$ is modified according to the prescription of Völk *et al.* [102], using the parameter ϵ. For $\epsilon = 0$ (solid line) the Alfvén speed is taken to be 1/50 times the particle speed. For $\epsilon = 1/30$ (dotted line), $\epsilon = 1/10$ (dashed line) and $\epsilon = 1/3$ (dot-dashed line), the Alfvén speed is set to zero.

the nonlinear calculations in the model for this coefficient. To this end, Völk *et al.* [102] introduced a simple prescription: setting $v_A = 0$, they assumed $\hat{D}_{\mu\mu}$ to be constant for $|\mu| < \epsilon$ and retained the quasilinear expression for $|\mu| \geq \epsilon$. For various values of ϵ, the resulting coefficient is shown in Figure 2.1. Two remarks should be made on this procedure. Firstly, the importance of the $\mu \approx 0$ region is larger for larger q. At $q = 1$ there is no reduction in $\hat{D}_{\mu\mu}$, which then corresponds to isotropic diffusion. Secondly, the difference between this procedure and the alternative of taking $\epsilon = 0$ and leaving v_A finite is significant only for small q, i.e. in that part of parameter space in which the precise dependence of $\hat{D}_{\mu\mu}$ at $\mu \approx 0$ is in any case less important. For $q = 2$, setting $v_A = 0$ and $\epsilon = \epsilon_0$ is equivalent to setting $v_A = \epsilon_0 v$ and $\epsilon = 0$. As the results presented below are not very sensitive to the value of ϵ, it is justified, for the present, to adopt this simple prescription, and restrict consideration to the representative forms of $\hat{D}_{\mu\mu}$ shown in Figure 2.1.

2.3 The Collision Operator for Large-Angle Scattering

The quasi-linear theory is restricted to levels of turbulence which are much lower than those encountered in practice, so that pitch-angle diffusion as described above is not necessarily a good model for the transport of charged particles close to relativistic shock fronts. However, there is no theory of strong turbulence which enables one to compute scattering operators, so that the only alternative is to use semi-empirical forms motivated by the results of computer simulations. One salient property of these simulations remarked upon by Zachary [107] and Quest [82] is large-angle scattering. Consequently, it is of interest to investigate the effect of such a scattering operator on Fermi acceleration. Of course, there is even more freedom available in choosing a

model of the large-angle scattering operator than is the case for small-angle scattering, so that severe restrictions must be placed on the parameter range to be investigated.

As a mathematical model we choose the Boltzmann collision operator in the test particle approximation. This operator has been widely studied in the theory of radiative transfer and neutron transport [23]. Allowing for the possibility of absorption as well as scattering, it reads:

$$\left(\frac{\partial f}{\partial t}\right)_{\text{collisions}} = \nu_\ell \left\{ \omega \left[\int_{-1}^{+1} d\mu' \, f(\mu') p(\mu, \mu') \right] - f(\mu) \right\}, \qquad (2.12)$$

where ν_ℓ is the frequency of (large-angle) scattering or absorption events, $p(\mu, \mu')d\mu$ is the probability that in a single scattering a particle with pitch μ' is scattered into the range $d\mu$ around μ and ω is the single scattering albedo [17], which is the probability that an elementary interaction is a scattering and not an absorption event. From these definitions as probabilities, one has the additional properties:

$$\int_{-1}^{+1} d\mu \, p(\mu, \mu') = 1, \qquad (2.13)$$

$$p(\mu, \mu') \geq 0 \qquad (2.14)$$

and

$$\omega \leq 1. \qquad (2.15)$$

In the following, we shall usually be interested in the case $\omega = 1$, i.e. pure scattering, in order to model the effects of strong turbulence on charged particles. Further it will be assumed that the phase function for the distribution of scattered particles is a function of only the angle Θ between the initial and final velocity vectors; $p(\mu, \mu') = p(\cos\Theta)$. It is then convenient to represent

$p(\cos\Theta)$ in terms of the Legendre polynomials:

$$p(\cos\Theta) = \sum_{n=0}^{\infty}(2n+1)\sigma_n P_n(\cos\Theta). \tag{2.16}$$

One then has

$$p(\mu,\mu') = \sum_{n=0}^{\infty}(2n+1)\sigma_n P_n(\mu)P_n(\mu') \tag{2.17}$$

[17, §48].

This phase function is conventionally said to describe "anisotropic scattering". However, the anisotropy which it describes is restricted. Although the phase function may depend on the scattering angle, it must, for this representation, be independent of the direction of propagation of the incoming particle. In modelling the transport of charged particles, it may become necessary to relax this restriction, in order to allow for the presence of a background magnetic field. Then, instead of equation (2.17), one would write

$$p(\mu,\mu') = \frac{1}{2}\sum_{m,n}\sqrt{(2m+1)(2n+1)}\,P_m(\mu)\sigma_{mn}P_n(\mu'), \tag{2.18}$$

where σ_{mn} must be a symmetric matrix to fulfil the principle of detailed balance.

However, for the present, we retain the simpler description and further model it in terms of a single parameter, using the Henyey/Greenstein [33] phase function:

$$p(\cos\Theta) = \frac{1}{2}(1-g^2)(1+g^2-2g\cos\Theta)^{-3/2} \tag{2.19}$$

in which the parameter g is just the mean of the cosine of the scattering angle. Differentiating the generating function of the P_n,

$$(1-2g\cos\Theta+g^2)^{-1/2} = \sum_{k=0}^{\infty} g^k P_k(\cos\Theta) \tag{2.20}$$

with respect to g, multiplying the result by $2g$ and adding it to equation (2.20) yields, by comparison with equation (2.19),

$$p(\cos\Theta) = \frac{1}{2}\sum_{n=0}^{\infty}(2n+1)g^n P_n(\cos\Theta). \tag{2.21}$$

Together with (2.12–2.17) this then leads to the equation

$$\left(\frac{\partial f}{\partial t}\right)_{\text{collisions}} = \nu_\ell C_\ell f. \tag{2.22}$$

The large-angle scattering operator is

$$C_\ell = -\left[1 - \omega\int_{-1}^{+1} d\mu' K(\mu,\mu')\circ\right] \tag{2.23}$$

where the more conventional notation $K(\mu,\mu)$ is used for the kernel:

$$K(\mu,\mu') = \sum_{n=0}^{\infty} g^n \mathcal{P}_n(\mu)\mathcal{P}_n(\mu'), \tag{2.24}$$

which is just equal to the phase function $p(\mu,\mu')$. Here, we have introduced the normalized Legendre polynomials $\mathcal{P}_n$, related to the standard P_n's by

$$\mathcal{P}_n(\mu) = \sqrt{\frac{2n+1}{2}}\,P_n(\mu). \tag{2.25}$$

The stationary transport equation including both pitch-angle diffusion and large-angle scattering is, therefore,

$$\Gamma(u+v\mu)\frac{\partial f}{\partial z} = \nu_s C_s(f) + \nu_\ell C_\ell(f) + S(f). \tag{2.26}$$

CHAPTER III

Relativistic Shock Fronts in Fluids

Relativistic effects can be important at shock fronts for two distinct reasons. On the one hand, the post shock temperature can be so high that the thermal motion of individual particles approaches the speed of light. On the other hand, it is possible that so much energy is released into a region containing fluid that the subsequent expansion proceeds at a bulk speed approaching that of light. It is certainly possible for the former effect to arise when all bulk velocities are quite modest. For example, a hot plasma in which the pressure is provided predominantly by photons is always relativistic in this sense, and behaves as a gas whose ratio of specific heats is 4/3. If the mass density in such a plasma is dominated by atoms or ions, there exists a sound velocity which is determined by the pressure of the photons and the inertia of the ions and which can be small compared to the speed of light. In the subsonic zone downstream of a strong shock front in such a plasma, the bulk speed is, of course, less than this sound speed, whereas the upstream fluid speed (provided it is still nonrelativistic) is equal to seven times the downstream speed. Such conditions can occur in several astrophysical situations e.g. in the break-out phase of a supernova shock front, or in a standing shock in an accretion flow onto a neutron star, or in the radiation dominated phase of the early universe [62,11,46]. In contrast, it does not seem possible for a relativistic bulk flow to be thermalized by a shock front without producing thermal velocities which

are also relativistic. As a consequence, it is essential to consider the fully relativistic equation of state of a plasma before proceeding to investigate the possible jump conditions.

Astrophysical plasmas are rarely observed to be in full thermodynamic equilibrium. Indeed, the time required for a diffuse interplanetary or interstellar plasma to relax to such a state by two-body collisions is normally prohibitively long. On the other hand, some components of a plasma may reach a state close to that of equilibrium by means of collective interactions, but this does not mean that the individual components necessarily reach equilibrium with each other. The jump conditions for relativistic shocks which are derived in this section depend sensitively on exactly how the upstream kinetic energy is converted into thermal energy in the various components of the downstream gas. In the absence of any detailed theoretical model, the best approach is to investigate several possibilities. Four will be considered:

1. The downstream plasma reaches full thermodynamic equilibrium.

2. The electrons in the downstream region remain cold, the pressure being provided by the ions.

3. The ions in the downstream region remain cold and electron pressure dominates.

4. Electron–positron pairs are produced at the shock front and they, together with the original electrons, provide the pressure.

Each of these options is a plausible model of the potentially complicated effects of a collisionless shock front [98]. The first assumes that collective processes in the shock are effective in coupling the electron temperature to that of the ions. The second assumes that the carriers of kinetic energy in the upstream zone —

which are the ions — retain this energy and thermalize it amongst themselves. The third assumes the opposite, and might occur if the collective processes which mediate the shock are ones which heat predominantly light particles — electrostatic modes, for example. The fourth takes account of the fact that the electron temperature behind a relativistic shock can easily attain values in the MeV range, in which case significant numbers of electron–positron pairs could be produced.

For each of these possibilities, the equation of state of a plasma consisting of a mixture of fully ionized hydrogen and helium, together with the associated electrons, is investigated. (The third and fourth cases are identical for this purpose.) The main factor complicating the relativistic equation of state is that the mean particle energy is no longer directly proportional to the temperature, as it is in the nonrelativistic case, necessitating a numerical approach. Following this, the jump conditions for a strong shock are derived by demanding continuity of the particle, momentum and energy fluxes at the shock front. The possibility of electron–positron pair creation is included by relaxing the equation of continuity of the particle flux.

3.1 Equation of State

Assuming that the fluid under consideration behaves as a classical ideal gas, the phase-space density of the fluid particles f_i (where i labels the constituents of the fluid) is simply given by

$$f_i \propto \exp(-E/T_i) \tag{3.1}$$

[96], where T_i is the temperature associated with the i'th constituent (Boltzmann's constant is set equal to unity) and $E = p^0$ is the particle energy. The components of the stress-energy tensor $T^{a,b}$ for each constituent are related to

the phase-space density by

$$T^{a,b} = \int \frac{d^3p}{E} p^a p^b f_i. \tag{3.2}$$

This tensor is diagonal provided, as assumed here, that f_i is isotropic in the frame considered. The total energy density e_i (including the rest-mass) of the i'th component is the element $T^{0,0}$ and the pressure P_i is equal to each of the other diagonal elements. The equation of state follows in a straightforward manner by elimination of the constant of proportionality in equation (3.1). Denoting this constant by A, one has

$$e_i = 4\pi A \int_0^\infty dp\, p^2 E \exp(-E/T_i) \tag{3.3}$$

$$P_i = \frac{4\pi}{3} A \int_0^\infty dp\, \frac{p^4}{E} \exp(-E/T_i), \tag{3.4}$$

and for the number density n_i:

$$n_i = 4\pi A \int_0^\infty dp\, p^2 \exp(-E/T_i). \tag{3.5}$$

With the use of the relation $E = \sqrt{m_i^2 + p^2}$ (m_i is the rest-mass of the particles of the i'th constituent) and some standard integrals, the equation of state for a single component is obtained:

$$e_i = m_i n_i R(m_i/T_i) \tag{3.6}$$

where the function R is defined according to:

$$R(z) = \frac{3}{z} + \frac{K_1(z)}{K_2(z)}, \tag{3.7}$$

with $K_\nu(z)$ the modified Bessel function of order ν. In addition, the ideal gas law

$$P_i = n_i T_i \tag{3.8}$$

follows from equations (3.4) and (3.5). The fluid we wish to investigate is composed of fully ionized helium and hydrogen, together with the associated

electrons. Summing over these, one has for the total pressure P, energy density e and "rest-mass density" ρ:

$$P = \sum n_i T_i \tag{3.9}$$

$$e = \sum m_i n_i R(m_i/T_i) \tag{3.10}$$

$$\rho = \sum m_i n_i. \tag{3.11}$$

(Note that the Einstein summation convention does not apply in this chapter.) The equation of state for the fluid as a whole is best presented by defining a quantity Γ_{ad}, in analogy with the ratio of specific heats [9]:

$$P = (\Gamma_{ad} - 1)(e - \rho). \tag{3.12}$$

Three cases are of interest: equilibrium ($T_i = T$, for all i), ion pressure ($T_H = T_{He} = T$, $T_e = 0$) and electron pressure ($T_H = T_{He} = 0$, $T_e = T$). Γ_{ad} can then be found from equations (3.6–3.11), given the composition and either the energy density, or the pressure, or the temperature T. Finding the jump conditions requires one to evaluate Γ_{ad} as a function of the average Lorentz factor of the fluid e/ρ. This involves solving (3.10) numerically to find T (note that $R(\infty) = 0$). Since the right hand side of (3.10) is a monotonic function of T, there is no difficulty in finding a suitable algorithm. Then, using the pressure computed from (3.9) and (3.8) enables Γ_{ad} to be evaluated by means of equation (3.12).

In the nonrelativistic and ultrarelativistic limits it is possible to simplify the equation of state considerably. At low temperatures, the function R of equation (3.7) may be evaluated using the asymptotic expansions of the modified Bessel functions for large argument:

$$R(z) \to 1 + \frac{3}{2z} \qquad \text{as } z \to \infty \tag{3.13}$$

Thus, not only is the partial pressure of each constituent of the gas proportional to the temperature (equation 3.8) but the contribution to the energy density fulfills an equally simple relation:

$$e_i \approx n_i m_i + \frac{3}{2} n_i T_i. \tag{3.14}$$

$$= n_i m_i + \frac{3}{2} P_i \tag{3.15}$$

Because the definition of the ratio of specific heats in equation (3.12) has been chosen to exclude the rest mass contribution to the energy density, one obtains *independent of* T_i *and* n_i the value $\Gamma_{ad} = 5/3$, as expected for a nonrelativistic, monatomic gas.

In the opposite limit of very high temperature, the expression for R may be simplified by expanding the modified Bessel functions for small values of the argument:

$$R(z) \approx 1 + \frac{3}{z} \qquad \text{for } z << 1 \tag{3.16}$$

and the resulting energy density is given by

$$e_i \approx 3 n_i T_i. \tag{3.17}$$

$$= 3 P_i \tag{3.18}$$

This time, one obtains — again *independent of* T_i *and* n_i — the value $\Gamma_{ad} = 4/3$, appropriate for a gas of ultrarelativistic particles. In a similar manner, one may obtain Γ_{ad} for a gas composed of nonrelativistic ions and ultrarelativistic electrons at equal temperature. If just protons and electrons are present, the result of applying both approximations (3.13) and (3.16) is $\Gamma_{ad} = 13/9$.

Figure 3.1 shows the results of numerical calculations of the equation of state. The quantity Γ_{ad} tends to the nonrelativistic value of 5/3 for a monatomic gas in each of the three cases investigated. At higher values of the

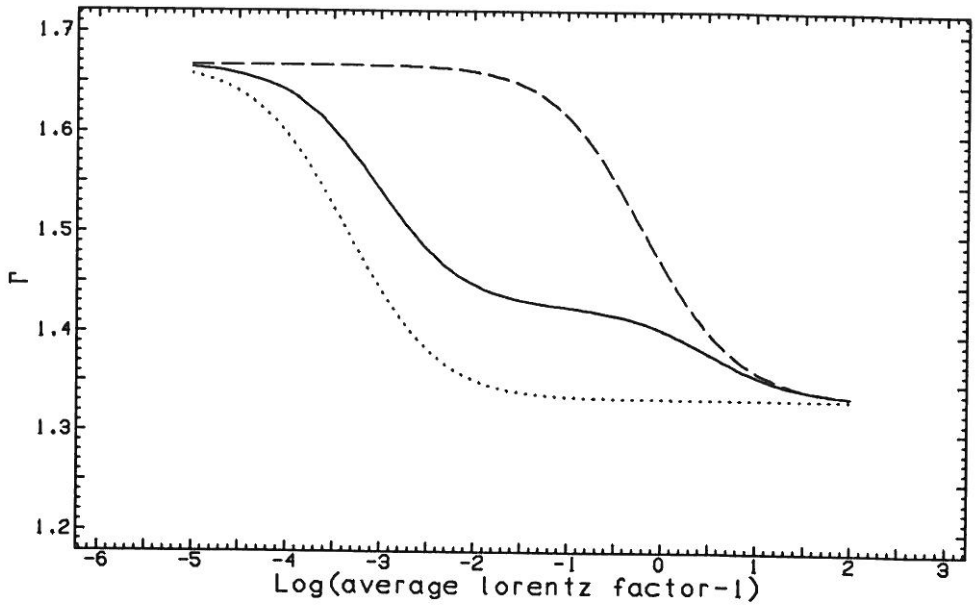

Figure 3.1: The equation of state of a gas consisting of fully ionized hydrogen and helium (25% by mass). Plotted is the ratio of specific heats, as defined in equation (3.12), as a function of the average Lorentz factor e/ρ. The abscissa has been chosen as the logarithm (to base 10) of the average Lorentz factor minus 1, to show the nonrelativistic regime in detail. Three cases are shown: thermal equilibrium (solid line), electron pressure only (dotted line) and ion pressure only (dashed line).

average Lorentz factor e/ρ the value of Γ_{ad} for the gas dominated by electron pressure falls off first, reaching the value 4/3 appropriate for an ultrarelativistic gas well before the average Lorentz factor (always evaluated for the gas as a whole) significantly exceeds unity. Such behaviour is easily understood, because the Lorentz factor of the *electrons*, which determines Γ_{ad} in this case, is much larger than the average Lorentz factor of the entire fluid. A similar fall off occurs in the case of full thermodynamic equilibrium. However, at moderate values of the average Lorentz factor, nonrelativistic ions contribute to the pressure, so that a plateau region is reached where $\Gamma_{ad} \approx 13/9$. Only when the ions themselves become relativistic does Γ_{ad} tend to the value 4/3. If the pressure is supplied by ions alone, the result is similar in form to that obtained when only electron pressure is present. However, the curve is shifted to higher Lorentz factors by a factor of roughly 2000.

Figure 3.2 shows essentially the same as Figure 3.1, except that the temperature found by a numerical solution of equation (3.12) is plotted in the abscissa. As the temperature is given in units of the electron rest mass, it can now clearly be seen that the fall off of the curve describing the case of electron pressure occurs when these particles become relativistic.

3.2 Jump Conditions

The equations of hydrodynamics can be expressed as the vanishing divergence of the stress-energy tensor:

$$T^{ab}{}_{;b} = 0. \tag{3.19}$$

From a knowledge of the explicit form of T^{ab} in the fluid frame it is straightforward to write down this tensor in an arbitrary frame in terms of the four-

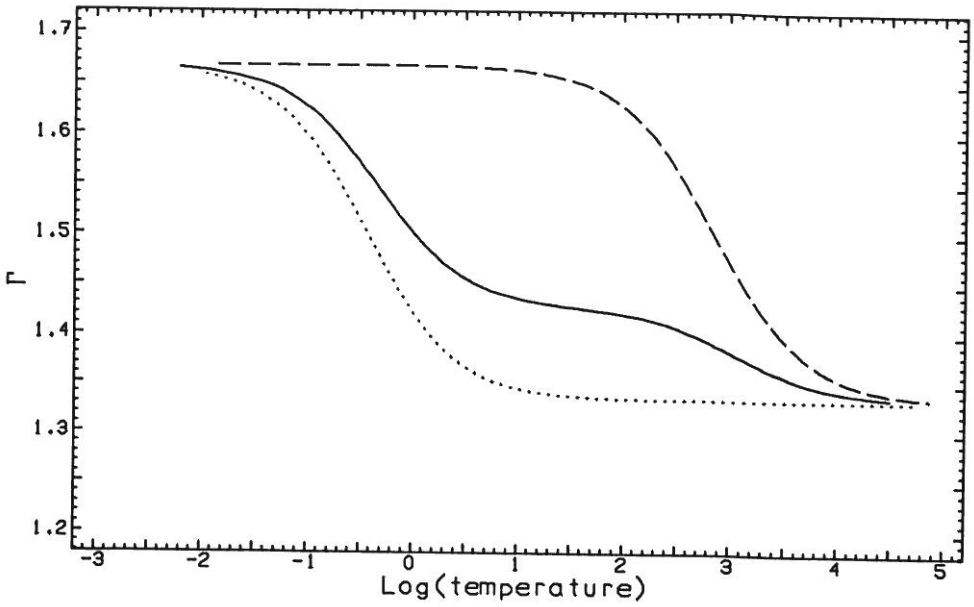

Figure 3.2: As in Figure 3.1, but with the logarithm of the temperature in units of the electron rest mass as the abscissa.

velocity U^a of the fluid:

$$T^{ab} = wU^aU^b + Pg^{ab}, \tag{3.20}$$

[56] where g^{ab} is the metric tensor (signature $-+++$) and w is the enthalpy density measured in the fluid frame: $w = e + P$.

Integrating equation (3.19) over a volume element which is contained between two surfaces, one just in the region upstream of a shock front and one just in the downstream region and applying Gauss' theorem leads to equations for the continuity of the energy and momentum fluxes across the shock. Placing the shock in the x–y plane, and taking both the upstream and downstream fluid velocities along the z–axis (i.e. $U^a = (U^0, 0, 0, U_z)$) gives

$$\left[wU_zU^0\right] = 0 \tag{3.21}$$

$$\left[wU_z^2 + P\right] = 0, \tag{3.22}$$

where the notation $[x]$ means the difference in the quantity x measured just

upstream and just downstream of the shock front. These equations can be supplemented by one describing the conservation of particle flux across the front. However, since we wish to allow for the possibility of the production of electron–positron pairs at the shock front itself, such an equation can be valid only for the ions and their associated electrons:

$$[n_i U_z] = 0. \qquad \text{(for conserved constituents)} \tag{3.23}$$

The rest-mass density associated with such conserved particles will be denoted by ρ_- (upstream) and ρ_+ (downstream). Then the rest-mass density ρ_{pairs} of particles created at the shock can be conveniently parameterized by the quantity

$$\eta = \frac{\rho_+}{\rho_+ + \rho_{pairs}} \tag{3.24}$$

which lies between 1 (no pairs) and 0 (pairs dominate the rest-mass density). Equations (3.21), (3.22) and (3.23) can be simplified by the introduction of the following notation: let the quantity ϕ be defined by

$$U^0 = \cosh\phi. \tag{3.25}$$

Then one has

$$U_z = \sinh\phi. \tag{3.26}$$

Further, using again the suffix $\pm$ to indicate upstream and downstream, the fluid velocity is

$$u_\pm = \tanh\phi_\pm \tag{3.27}$$

In terms of the energy per unit rest mass $\bar{e}_- = e_-/\rho_-$ and $\bar{e}_+ = e_+/(\rho_+ + \rho_{pairs})$ (we assume that pairs are present only in the downstream plasma) and the

similarly defined pressure per unit rest mass $\bar{P}_{\pm}$, one obtains

$$\rho_+ \sinh\phi_+ = \rho_- \sinh\phi_- \tag{3.28}$$

$$(\bar{e}_+ + \bar{P}_+)\sinh^2\phi_+ + \bar{P}_+ = \eta\frac{\rho_-}{\rho_+}\left[(\bar{e}_- + \bar{P}_-)\sinh^2\phi_- + \bar{P}_-\right] \tag{3.29}$$

$$(\bar{e}_+ + \bar{P}_+)\sinh\phi_+ \cosh\phi_+ = \eta\frac{\rho_-}{\rho_+}\sinh\phi_- \cosh\phi_-(\bar{e}_- + \bar{P}_-). \tag{3.30}$$

Elimination of ρ_+/ρ_- leads, after a little manipulation, to

$$\bar{w}_+ \cosh\phi_+ = \eta\bar{w}_- \cosh\phi_- \tag{3.31}$$

and

$$(\bar{w}_+ \cosh^2\phi_+ - \bar{e}_+) = \eta\bar{e}_- \sinh\phi_+ \sinh\phi_- \left(1 + \frac{\bar{P}_- \coth^2\phi_-}{\bar{e}_-}\right), \tag{3.32}$$

where $\bar{w}_{\pm} = \bar{e}_{\pm} + \bar{P}_{\pm}$. The last term on the right-hand side of equation (3.32) can be neglected if one restricts one's consideration to strong shocks, i.e. to shocks in which the upstream pressure is negligible. This approximation may be extended by assuming the upstream medium is cold, in which case the gas possesses only that energy attributable to its rest mass: $\bar{e}_- = 1$. Then, eliminating $\cosh\phi_+$, one has

$$\cosh^2\phi_- = \frac{\bar{w}_+^2(\bar{e}_+^2 - \eta^2)}{\eta^2(\bar{e}_+^2 - \eta^2 - \bar{P}_+^2)} \tag{3.33}$$

which is a generalization of the relation given by Peacock [78].

Alternatively, one may obtain from equations (3.31) and (3.32) the relation

$$\bar{e}_+ = \cosh\phi_- \cosh\phi_+ - \eta\sinh\phi_- \sinh\phi_+ \tag{3.34}$$

$$= \cosh(\phi_- - \phi_+) \qquad (\text{for } \eta = 1) \tag{3.35}$$

valid for strong shocks which do not produce pairs. The right-hand side of this expression is just the Lorentz factor associated with the relative velocity of the upstream fluid with respect to the downstream fluid. Thus, when $\bar{e}_- = 1$ and

pairs are absent, the energy per particle is constant across the shock, as seen from the frame of the downstream fluid [35,9].

For a given upstream velocity u_-, equation (3.33) must be solved numerically to give the downstream parameters. The procedure is as follows: u_- determines $\cosh\phi_-$ through the relation $\cosh\phi_- = (1-u_-^2)^{-1/2}$. The right-hand side of (3.33) is a function of the single parameter $\bar{e}_+$ — which is termed the average Lorentz factor in the previous section — since the pressure $\bar{P}_+$ is given through the equation of state $\Gamma_{ad}(\bar{e}_+)$ and the relation (3.12). A root finding algorithm can therefore be used to find $\bar{e}_+$. By means of equation (3.31), which specializes to

$$\cosh\phi_+ = \frac{\eta}{\bar{w}_+}\cosh\phi_-, \tag{3.36}$$

one finds the downstream velocity u_+.

Before proceeding to discuss the results of the numerical solutions, it is instructive to consider the two limits in which the equation of state takes on a simple form. In the absence of pair production ($\eta = 1$) and at low temperatures, the use of equation (3.15) enables equations (3.33) and (3.31) to be written

$$u_-^2 = \frac{16}{3}\bar{P}_+ \tag{3.37}$$

and

$$u_+^2 = \frac{1}{3}\bar{P}_+ \tag{3.38}$$

from which one readily deduces the well-known jump conditions for a nonrelativistic strong shock in a gas of $\Gamma_{ad} = 5/3$:

$$u_- = 4u_+. \tag{3.39}$$

The ultrarelativistic case is best considered without imposing the restriction to strong shocks. The equation of state (3.18) can then be applied in both the

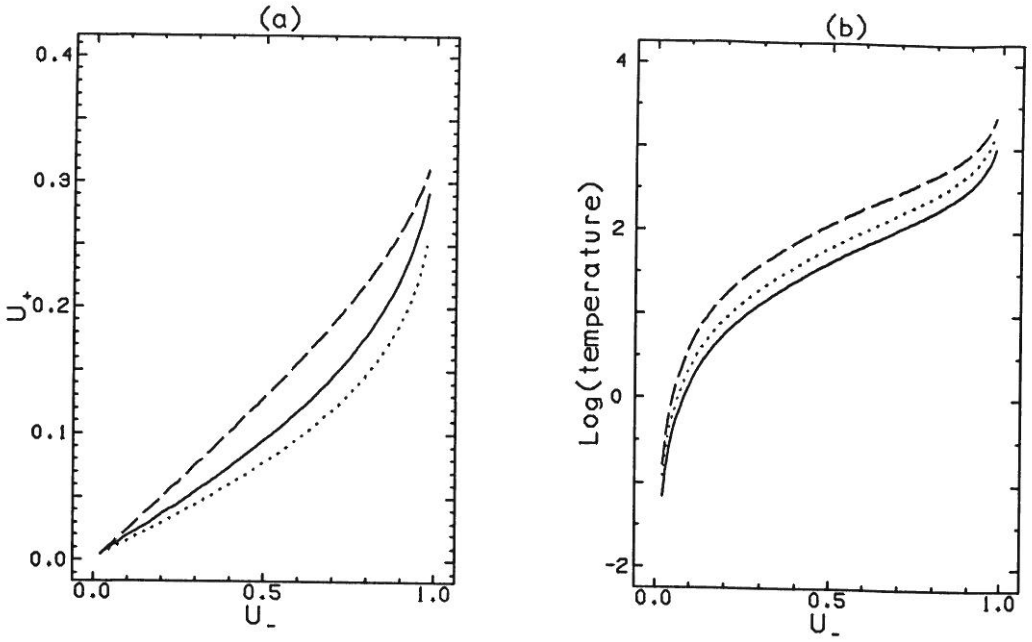

Figure 3.3: a) The downstream velocity u_+ as a function of the upstream velocity u_- for a strong shock in an ideal gas under the assumption that the pressure is provided either by the electrons alone (dotted line), or by the ions alone (dashed line), or that the gas is in full thermodynamic equilibrium (solid line). b) The logarithm of the temperature (in units of the electron rest mass) behind the shock front. Electrons are relativistic for $\log(T) > 0$, whereas ions require $\log(T) > 3$. When both ions and electrons contribute to the pressure, a lower temperature is achieved behind the shock front.

upstream and downstream regions. Returning to equations (3.31) and (3.32), one finds, after a straightforward calculation,

$$u_- u_+ = \frac{1}{3}. \tag{3.40}$$

This is the simplest jump condition available which is valid in the relativistic regime. It is independent of the composition of the plasma and the presence or absence of pair production; as such, it has been used to illustrate the basic properties of acceleration at relativistic shocks [49]. The case of a strong shock arises when the upstream velocity tends to the velocity of light $u_- \to 1$. The downstream velocity is then $u_+ = 1/3$.

The jump conditions as calculated numerically are shown in Figure 3.3.

Without pair production ($\eta = 1$), three cases are considered. Figure 3.3a shows the downstream velocity as a function of the upstream velocity for each of these. At very low upstream velocities, the downstream medium remains nonrelativistic and the jump conditions are given by equation (3.39). However, as can be seen from Figure 3.3b, where the temperature of the downstream medium is shown, the electrons quickly become relativistic as the upstream velocity is increased. There follows a region in which the compression ratio of the shock is 1/7, when only electron pressure is included. This corresponds to the result obtained for a gas with a relativistic equation of state, equation (3.18), in nonrelativistic motion. As can be seen from Figure 3.3b, the ions start to become relativistic only when the upstream velocity approaches unity. Consequently, when only ion pressure is present, there exists a large region of parameter space $0 < u_- < 1/2$ within which the compression ratio is 4, as in the case of a nonrelativistic monatomic gas. If the pressure in the downstream medium is provided by the electrons alone, the equation of state is "soft", leading to a higher compression ratio than is the case when the ions contribute to the pressure. The case in which complete thermodynamic equilibrium is assumed is intermediate in both the softness of the equation of state (Figure 3.1) and the resulting compression ratio. As the upstream velocity tends to unity, each of the three curves tends to the limit of the strong relativistic shock $u_+ \to 1/3$.

The results of permitting various numbers of electron–positron pairs to be created in the shock front is shown in Figure 3.4. The equation of state remains the same as that obtained when only electron pressure is present. Nevertheless, Figure 3.4 shows that except for very high upstream speeds, there is a marked increase in the compression ratio as the number of pairs is raised. This can be explained as the result of having more particles available

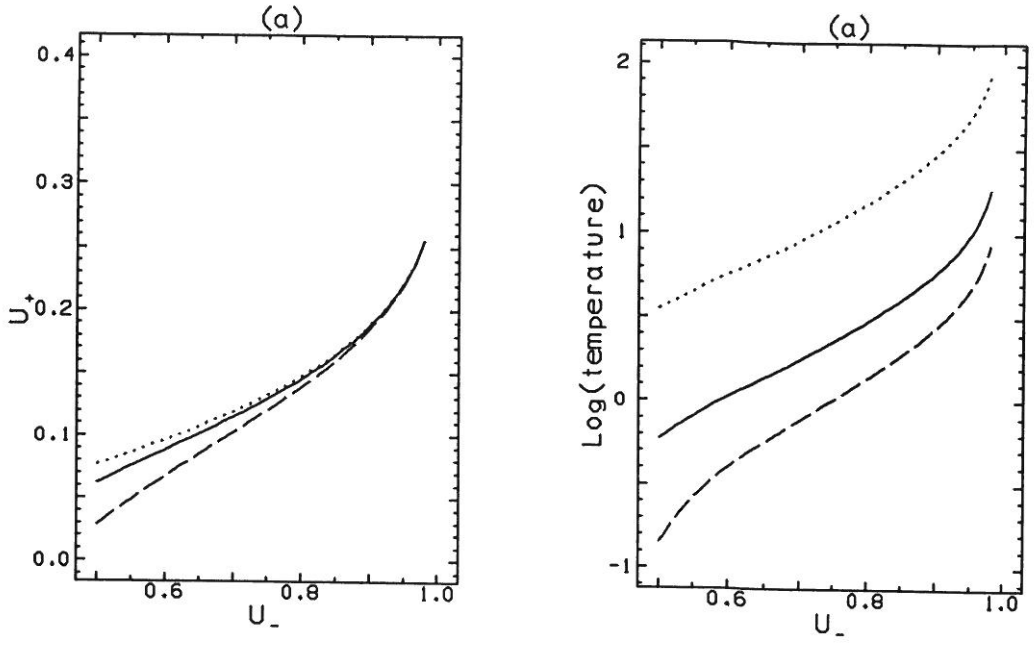

Figure 3.4: a) The downstream velocity u_+ as a function of the upstream velocity u_- for a strong shock under the assumption that the pressure is provided by the electrons and electron–positron pairs created at the shock front. The number of pairs is controlled by η of equation (3.24). The cases $\eta = .99$ (dotted line), 0.95 (solid line) and 0.9 (dashed line) are shown. b) The logarithm of the temperature (in units of the electron rest mass) behind the shock front. Pairs are very effective at supporting the shock front, so that in their presence a much lower post-shock temperature is obtained.

to transport away from the shock the energy and momentum fluxes brought in from upstream. A lower fluid velocity then suffices. Furthermore, since the density is increased by the presence of pairs, a lower temperature is obtained behind the shock, as may be seen in Figure 3.4b. Once again, as the upstream velocity tends to the speed of light, the limit of an ultrarelativistic strong shock is approached, independent of the number of pairs produced.

In summary, a variety of jump conditions may occur at a strong relativistic shock. If electron pressure dominates, a large compression ratio is obtained — as a result of the soft equation of state. The production of pairs at the shock front further increases the compression ratio. The smallest compression ratios are obtained when the pressure is dominated by the ions. Thermody-

namic equilibrium produces results intermediate between these two extremes. As the upstream speed tends to that of light, *all* cases tend to that of a strong ultrarelativistic shock with $u_- = 1$ and $u_+ = 1/3$.

CHAPTER IV

The Q_J Method

The stationary transport equation (2.26) is an equation for the distribution function $f(p, \mu, z)$ in two independent variables z and μ. The variable p enters as a parameter, since neither the Liouville operator, §2.1 nor the collision operators considered in §2.2 and §2.3 operate on p. Depending on the character of these operators, the equation is either a partial differential equation or an integro-differential equation. A standard method of attacking the problem of solving such equations is the separation of variables. Fortunately, this is always possible in the problem to be treated here and, as is usually the case, the technique reduces the equation to an eigenvalue problem. In the theory of the transfer of neutrons in fission reactors this technique was used by Case [15] in order to solve the so-called "single-speed transport equation". The collision operator for neutrons is that of large-angle scattering (2.3) for which, as is discussed below, the eigenfunctions are singular. Thus the method came to be known as the "singular eigenfunction method". In the theory of radiative transfer, the same equation is obtained when the approximation of "grey" opacities is made, or when the medium gives rise only to coherent scattering of photons and not to absorption. Early work on solutions of this equation — including the celebrated Milne Problem [71] — employed the related technique of integral transforms [105,17].

In principle, the problem at hand can be solved by the singular eigen-

function method. The only generalization of the single-speed transport equation arises because we are interested in transport in a *moving* medium, whereas only stationary media have been considered in previous applications. However, to compensate for this complication, the present problem is in some ways simpler than that in which only the large-angle scattering operator appears. In particular, if the collision operator for pitch-angle diffusion is adopted — which will be the case for the major part of the investigation — the eigenvalue problem is a second-order differential equation of the Sturm type [40]. The eigenfunctions are then no longer singular, which renders feasible the task of expressing the solution as a finite sum over these functions. As is demonstrated in §4.1, this advantage remains even when the collision operator is modified to include a contribution from large-angle scattering.

Although the pitch-angle scattering operator results in a relatively simple eigenvalue problem, it does not appear possible to express the eigenfunctions in closed form. A direct numerical integration of the equation would, of course, be possible. However, it turns out that only a few eigenfunctions are required to represent the solution accurately, so that a Galerkin method is adequate. This method is described in detail in §4.2. It consists of expressing each eigenfunction as an expansion in "trial functions" plus a remainder, and then demanding that the remainder be orthogonal to the trial functions themselves [29]. The Galerkin method has one further advantage: if Legendre polynomials are used as the trial functions, much of the formalism is similar to that of the "P_N method" of radiative transfer [80]. Treatment of the large-angle scattering operator in terms of the Henyey–Greenstein phase function, equation (2.19), is then considerably facilitated.

Once the eigenfunctions have been found, the general solution of the

stationary transport equation with constant fluid speed u can be written down. For a shock front, one obtains the general solution in each half-space: the upstream region, and the downstream region. Boundary conditions can be imposed on these solutions at large distances from the shock. Thus, the requirement that the distribution not diverge far upstream of the shock limits those eigenfunctions which may be employed in expressing the solution in the upstream region, and a similar limitation can be found for the downstream solution. However, these conditions do not suffice to determine the solution completely. In addition, it is necessary to decide upon what happens to the distribution at the shock front itself.

The simplest condition — that the distribution be continuous across the shock front — is also the one with the strongest physical motivation. Whatever the collective processes are which succeed in thermalizing the energy of the upstream fluid as it passes through the shock front, it is unlikely that they are the same as those responsible for the scattering of energetic particles in the plasma. If, for example, an electrostatic potential barrier decelerates the upstream fluid, the potential drop must be of the order of the kinetic energy of an ion in the upstream fluid. An ultrarelativistic particle such as those considered here has, by assumption, a much higher energy, so that the slight acceleration or deceleration suffered by it on crossing the shock is negligible. Similarly, if waves operating at the ion-cyclotron resonance are responsible for the formation of the shock front (as is currently thought to be the case for parallel shocks [82]), these will have negligible effect on the ultrarelativistic particles because of the much smaller gyro-frequency which they possess.

Continuity of the distribution function across the shock front completes the specification of the problem. However, it is not an easy condition

to implement. Only when the momentum dependence of the distribution assumes a simple form does the problem become tractable. Since the scattering operator is independent of momentum, a power-law distribution in momentum will result if the boundary conditions far from the shock front can be formulated in a momentum independent manner and the matching condition at the shock front also does not introduce a momentum scale. This is the case for ultrarelativistic particles, for which $v = 1$, irrespective of the fluid velocities. It is also true provided all particles are much faster than the fluid $v >> u$.

Physically, a power-law solution means that no momentum scale has been introduced into the problem. One obvious momentum scale is that of a particle whose velocity equals the fluid speed (either downstream or upstream) and such particles may not be represented by a power-law distribution. In the application to relativistic fluid flows, the energetic particle velocity, being limited by that of light, is always comparable to the fluid velocity. Hence, a power-law solution can be found only for ultrarelativistic particles, and the treatment of §4.3 is restricted to this case. Suitable boundary conditions are discussed in §4.3, where the details of the matching procedure at the shock front are also presented. The problem is thus formulated as that of finding the power-law index of the distribution of accelerated particles, given the upstream and downstream fluid velocities and the nature of the scattering.

4.1 The Eigenfunction Expansion

Separating the variables in the stationary transport equation (2.26), leads to the general solution expressed in the form

$$f = \sum_{i=-\infty}^{\infty} g_i(p) Q_i^{\nu}(\mu) \exp(\Lambda_i z/\Gamma v), \tag{4.1}$$

where the $g_i(p)$ are arbitrary functions of momentum. The eigenvalues Λ_i and eigenfunctions $Q_i^\nu(\mu)$ are solutions of the equation

$$\nu_s \frac{\partial}{\partial \mu} \hat{D}_{\mu\mu} \frac{\partial}{\partial \mu} Q_i^\nu(\mu) + \nu_\ell \left[\omega \int_{-1}^{+1} d\mu' \, K(\mu, \mu') Q_i^\nu(\mu') \right] = \left[\Lambda_i(\nu + \mu) + \nu_\ell \right] Q_i^\nu(\mu), \qquad (4.2)$$

where $\nu = u/v$, is the ratio of the fluid speed to the particle speed. In this section, the explicit dependence on the velocity of the accelerated particles is retained, since the eigenfunction method finds application to low energy particles in the solar wind [47]. Only in §4.3 is it essential to specialize to the case $\nu = u$. The boundary conditions to be imposed on equation (4.2) are that $\hat{D}_{\mu\mu} \partial Q_i^\nu(\mu)/\partial\mu = 0$ at $\mu = \pm 1$. Since the pitch-angle diffusion coefficient itself is zero at these end points, the boundary condition amounts to a regularity condition on the eigenfunctions.

4.1.1 Pitch-Angle Diffusion

When only pitch-angle diffusion is considered ($\nu_\ell = 0$), equation (4.2) is a second-order linear differential equation of the Sturm type, although it is not the most commonly encountered case because the weighting function $(\nu+\mu)$ changes sign within the interval under consideration ($-1 < \mu < 1$) for particles which move faster than the fluid ($|\nu| < 1$). Richardson [84] has called this the 'Polar Case' (see also [40]). There are an infinite number of discrete eigenvalues which occur in pairs $\Lambda^{(\pm i)}$ such that $\Lambda^{(i)} > 0$ and $\Lambda^{(-i)} < 0$, for $i = 1, \ldots \infty$. The only limiting points are at $\pm\infty$. In addition, there is the eigenvalue $\Lambda^{(0)} = 0$, with the eigenfunction $Q_0(\mu)$ =constant. The eigenfunctions are orthogonal on the interval $[-1, +1]$ with the weighting function $(\nu + \mu)$:

$$\int_{-1}^{+1} d\mu Q_i^\nu(\mu)(\nu + \mu) Q_j^\nu(\mu) = 0 \qquad [\text{for } i \neq j]\,. \qquad (4.3)$$

However, some care is necessary with the normalization. Rewriting equation (4.3) leads to

$$\int_{-1}^{+1} d\mu\, Q_i^\nu(\mu)(\nu+\mu)Q_j^\nu(\mu) = \frac{\nu_s}{\Lambda_i}\int_{-1}^{+1} d\mu\, Q_i^\nu(\mu)\frac{\partial}{\partial\mu}\hat{D}_{\mu\mu}\frac{\partial}{\partial\mu}Q_j^\nu(\mu) \quad (4.4)$$

$$= -\frac{\nu_s}{\Lambda_i}\int_{-1}^{+1} d\mu\, \hat{D}_{\mu\mu}\frac{\partial Q_i^\nu(\mu)}{\partial\mu}\frac{\partial Q_j^\nu(\mu)}{\partial\mu}, \quad (4.5)$$

valid for $i \neq 0$. For $i = j$, the integrand on the right-hand side of equation (4.5) is positive definite. Consequently, the most convenient normalization is

$$\int_{-1}^{+1} d\mu\, Q_i^\nu(\mu)(\nu+\mu)Q_j^\nu(\mu) = -\frac{\nu_s}{\Lambda_i}\delta_{ij}, \quad (4.6)$$

in which case

$$\int_{-1}^{+1} d\mu\, \hat{D}_{\mu\mu}\frac{\partial Q_i^\nu(\mu)}{\partial\mu}\frac{\partial Q_j^\nu(\mu)}{\partial\mu} = \delta_{ij}. \quad (4.7)$$

4.1.2 Large-Angle Scattering

When only large-angle scattering is included ($\nu_s = 0$) the eigenvalue problem is a homogeneous, linear, integral equation (in fact, a Fredholm equation of the second kind [66]):

$$\nu_\ell\omega\int_{-1}^{+1} d\mu'\, K(\mu,\mu')Q_i^\nu(\mu') = [\Lambda_i(\nu+\mu)+\nu_\ell]\, Q_i^\nu(\mu). \quad (4.8)$$

It can easily be shown that the eigenfunctions of this equation also satisfy the orthogonality relation (4.3). However, the spectrum of the eigenvalues is very different in this case. For values of Λ_i such that the factor on the right-hand side of equation (4.8) has a zero for $-1 \leq \mu \leq +1$ it is clear that a well-behaved eigenfunction does not exist. In fact, such values of Λ_i belong to the continuous spectrum of the equation. Defining

$$\lambda_i = \nu_\ell/\Lambda_i, \quad (4.9)$$

this range corresponds to

$$-1-\nu < \lambda < 1-\nu, \quad (4.10)$$

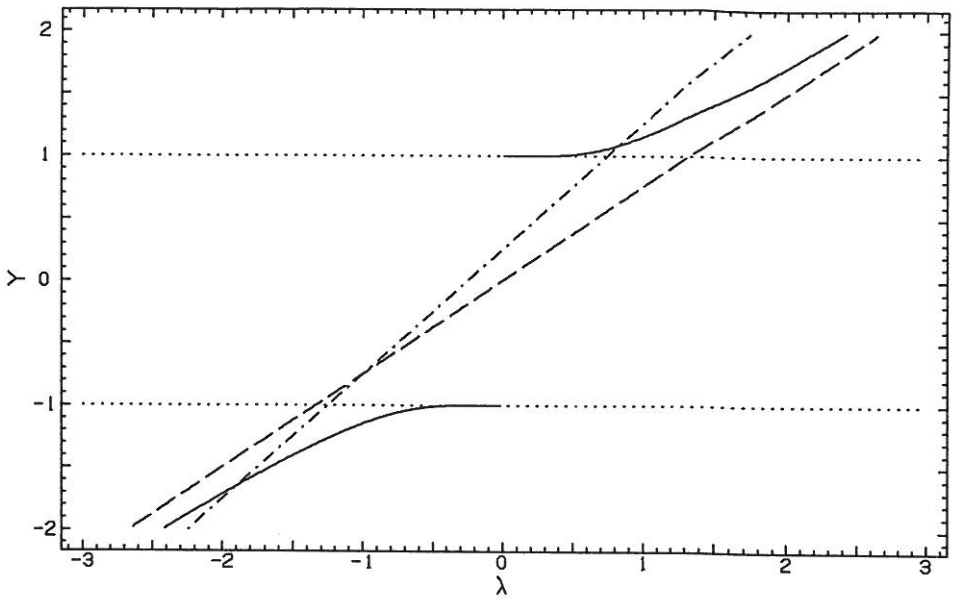

Figure 4.1: The graphical determination of the eigenvalues (λ_i) for the isotropic, large-angle scattering operator. The discrete eigenvalues are positioned at the intersections of the curves $y = y_1 = \nu + \lambda$ (dash–dotted line) and $y = y_2 = \coth(1/\omega\lambda)$ (solid lines) and the continuum lies between the intersections of $y = \nu + \lambda$ and the lines $y = \pm 1$ (dotted lines). The asymptote of y_2 is shown as a dashed line, the values $\nu = 1/4$ and $\omega = 3/4$ being used in this example.

where the suffix has been dropped in order to emphasize that the eigenvalue forms part of a continuum. The position of the continuum is independent of the kernel K and of the albedo ω.

In addition to the continuum, there also exists a discrete spectrum of eigenvalues. For the simple case of $K = 1/2$, for example, which corresponds to isotropic scattering ($g = 0$ in equation 2.19), the left-hand side of equation (4.8) is independent of μ. As the equation is homogeneous, one may choose the normalization of the eigenfunctions such that

$$\int_{-1}^{+1} d\mu \, Q_i^{\nu}(\mu) = 1. \tag{4.11}$$

The eigenfunctions are then simply

$$Q_i^\nu(\mu) = \frac{\nu_\ell \omega}{2\left[\Lambda_i(\nu+\mu)+\nu_\ell\right]}, \tag{4.12}$$

and the eigenvalues are found by inserting this expression into the normalization condition equation (4.11). This results in the equation

$$\begin{aligned} L(\lambda_i) &\equiv \frac{\lambda_i \omega}{2} \ln\left|\frac{\lambda_i+\nu+1}{\lambda_i+\nu-1}\right|, \\ &= 1 \end{aligned} \tag{4.13}$$

or, equivalently,

$$\lambda_i + \nu = \coth\left(\frac{1}{\omega\lambda_i}\right). \tag{4.14}$$

Considering the normalization condition for continuum eigenfunctions indicates the form they must assume:

$$Q^\nu(\mu) = \mathrm{P}\frac{1}{\lambda+\nu+\mu} + [1-L(\lambda)]\delta(\lambda+\nu+\mu), \tag{4.15}$$

where P denotes the Cauchy principal value. The solution of equation (4.14) is best considered graphically. Figure 4.1 shows the functions $y_1 = \lambda + \nu$ and $y_2 = \coth(1/\omega\lambda)$. The intersections of these two curves give the locations of the discrete eigenvalues λ_i. For large λ, $y_2 \to \omega\lambda$ and for $\lambda \to 0^\pm$, $y_2 \to \pm 1$. It can be seen from the figure that there are two discrete eigenvalues of opposite sign which are placed symmetrically with respect to the origin for $\nu = 0$. However, if the function y_1 and the asymptotes of y_2 have the same slope, which occurs for $\omega = 1$, then each of these roots goes to infinity when y_1 passes through the origin ($\nu = 0$). If y_1 has a positive intercept on the y–axis between 0 and 1 (i.e. $0 < \nu < 1$), only one of the roots goes to infinity, the positive one remaining finite. It can also be seen from Figure 4.1 that the discrete eigenvalues are always outside of the continuum, which lies between the intersections of y_1 with the lines $y = \pm 1$.

An infinite eigenvalue λ_i (i.e. $\Lambda_i = 0$) corresponds to an eigenfunction which is a constant, implying that a homogeneous, isotropic distribution is a solution of the stationary transport equation. Physically, this can happen only in the absence of absorption, as seen from the figure. Furthermore, if the solution to the transport equation is assumed to be stationary in the *fluid frame* ($\nu = 0$), an isotropic distribution is the only physically permitted solution in a semi-infinite domain, since all other eigenfunctions acquire a spatial dependence which diverges either as $z \to \infty$ or as $z \to -\infty$. Only the presence of a finite speed of the fluid in the frame in which the solution is stationary permits one to balance the transport due to scattering against advection by the fluid. Then, far upstream ($z < 0$ for $\nu > 0$) of a boundary or shock front, the solution tends to the eigenfunction corresponding to the single, discrete, positive eigenvalue and decays exponentially according to this eigenvalue.

Finding the discrete eigenvalues for more general forms of the kernel is somewhat complicated. However, it is interesting to note that the scattering phase function corresponds to a class of kernels about which much is known. Thus, because of the normalization property (2.13) and the symmetry $K(x,y) = K(y,x)$ the kernel belongs to the Schmidt-Hilbert class [23]. Furthermore, the kernel of equation (2.17) is degenerate provided the series may be truncated after a finite number of Legendre polynomials. Under these conditions, equation (2.18) may also be cast in degenerate form by diagonalizing the symmetric matrix σ_{mn}. One useful application of these properties is that they enable one to conclude [20] that the number of discrete eigenfunctions of the kernel (2.17) is less than or at most equal to the highest order polynomial used in the expansion.

4.1.3 The Mixed Operator

Whereas in the case of pitch-angle scattering the spectrum of eigenvalues is known to be purely discrete and in the case of large-angle scattering, a continuum is known to be present, little seems to be known about the spectral properties of mixed integral and differential operators. However, the singular eigenfunctions of §4.1.2 are associated physically with the unscattered component of a collimated beam of particles (or photons) injected into the medium. The exponential decay of this component along the path of the beam requires that the system have eigenvalues with the same spatial dependence: $\exp[(\pm z/(u+\mu)]$. These are indeed provided by the continuum for all $|\mu| \leq 1$. Once an amount of pitch-angle diffusion is introduced, however, there are no longer any unscattered particles in the medium. As soon as a particle enters, it begins to suffer a continuous deflection of its trajectory by the pitch-angle diffusion process. Thus, one concludes on physical grounds that the spectrum of the mixed operator need not contain a continuum, which leads one to suspect that the spectrum of the mixed operator is similar to that of pitch-angle diffusion i.e. purely discrete. Support for this suspicion can be found in the assertion of Kato [41] that continuum spectra are "rather unstable" as well as in the results of the numerical evaluation presented in §4.2.

4.1.4 The Diffusion Approximation

As noted in §4.1.2, a physically acceptable distribution function upstream of a boundary or shock front can be represented solely in terms of those eigenfunctions corresponding to positive eigenvalues. Far upstream, only the eigenfunction of the smallest positive eigenvalue $\Lambda_{i=1}$ survives. This function, therefore, must represent a physically acceptable distribution function. For

example, it may not possess a zero in the range $-1 \leq \mu \leq +1$.

In the diffusion approximation, it is assumed that the distribution function is everywhere close to isotropy. Applying this idea to the region far upstream of a shock front suggests that some information about the eigenvalue $\Lambda_{i=1}$ and its eigenfunction $Q^{\nu}_{i=1}(\mu)$ may be gained by a perturbative approach. This is indeed the case.

Assume that the eigenfunction in question can be approximated by

$$Q^{\nu}_{1}(\mu) \quad \propto \quad 1 + g(\mu) + h(\mu) \tag{4.16}$$

where

$$\int_{-1}^{+1} d\mu\, g(\mu) = \int_{-1}^{+1} d\mu\, h(\mu) = 0, \tag{4.17}$$

$$g(\mu) \sim O(\epsilon), \qquad h(\mu) \sim O(\epsilon^2) \quad \text{and} \quad \epsilon << 1. \tag{4.18}$$

Substituting into equation (4.2) (with $\nu_\ell = 0$), without making any additional assumptions concerning the ordering of the terms, immediately leads to the conclusion that Λ_1 cannot be larger than $\sim O(\epsilon)$. Collecting all the terms of $O(\epsilon)$ leads to an ordinary differential equation for g which can be integrated to give:

$$\nu_s \hat{D}_{\mu\mu} \frac{dg}{d\mu} = \Lambda_1 \left(\nu\mu + \frac{\mu^2}{2} \right) + \text{constant}. \tag{4.19}$$

According to the boundary conditions on the eigenfunction, the right-hand side of equation (4.19) must vanish for $\mu = \pm 1$. Therefore, one concludes that the ratio of velocities ν must be of order ϵ or smaller for the present approach to be valid. In this case, another integration yields:

$$g(\mu) \quad = \quad -\frac{\Lambda_1}{2\nu_s} \int_0^{\mu} d\mu' \frac{1 - \mu'^2}{\hat{D}_{\mu'\mu'}}. \tag{4.20}$$

which leads to:

$$Q_1^\nu(\mu) \;=\; 1 - \frac{\Lambda_1}{2\nu_s}\int_0^\mu d\mu' \,\frac{1-\mu'^2}{\hat{D}_{\mu'\mu'}}. \tag{4.21}$$

The constant of integration here is chosen from the constraint (4.17), assuming, for simplicity, that $\hat{D}_{\mu\mu}$ is an even function of μ.

Turning now to the equation for terms $O(\epsilon^2)$, this may be integrated once to give:

$$\nu_s \hat{D}_{\mu\mu}\frac{dh}{d\mu} = \Lambda_1\left[\nu\mu + \int_{-1}^{\mu} d\mu'\,\mu' g(\mu')\right] + \text{constant}. \tag{4.22}$$

Once again, the right-hand side must vanish at $\mu = \pm 1$, which leads this time to the requirement

$$\int_{-1}^{+1} d\mu'\,\mu' g(\mu') \;=\; 2\nu \tag{4.23}$$

and, hence, to an expression for the eigenvalue:

$$\Lambda_1 \;=\; 8\nu_s\nu\left[\int_{-1}^{+1} d\mu\,\frac{(1-\mu^2)^2}{\hat{D}_{\mu\mu}}\right]^{-1}. \tag{4.24}$$

These expressions provide a useful test of the Galerkin method described in §4.2 below. To express them in terms of the spatial diffusion coefficient κ, note that this coefficient relates the gradient of the particle density to the flux [24]. One then has:

$$\kappa \;=\; \nu_s\nu v^2/\Lambda_1. \tag{4.25}$$

4.2 Numerical Evaluation of the Eigenfunctions

The Galerkin method adopted here consists of writing the eigenfunctions in terms of a number of trial functions and a remainder. Using the first $N+1$ normalized Legendre polynomials as trial functions, one has

$$Q_i^\nu(\mu) \;=\; \left[\sum_{n=0}^{N} P_n(\mu) q_{ni}^\nu\right] + \mathcal{R}_i^\nu(\mu). \tag{4.26}$$

Now, the coefficients q_{ni}^{ν} are determined by imposing the requirement that the remainder $\mathcal{R}_i^{\nu}(\mu)$ be orthogonal to the trial functions $P_n(\mu)$. When substituted into equation (4.2), this results in an algebraic eigenvalue problem:

$$\sum_{n=0}^{N} S_{mn} q_{ni}^{\nu} = -\Lambda_i \sum_{n=0}^{N} W_{mn} q_{ni}^{\nu} \qquad [m = 0, \ldots N]. \tag{4.27}$$

The symmetric matrices S and W are defined by

$$S_{mn} = \nu_s \left[\int_{-1}^{+1} \mathrm{d}\mu \, \hat{D}_{\mu\mu} \frac{\mathrm{d}P_m(\mu)}{\mathrm{d}\mu} \frac{\mathrm{d}P_n(\mu)}{\mathrm{d}\mu} \right] + \nu_\ell \delta_{mn} (1 - \omega g^n) \tag{4.28}$$

and

$$W_{mn} = \int_{-1}^{+1} \mathrm{d}\mu \, (\nu + \mu) P_m(\mu) P_n(\mu), \tag{4.29}$$

where the form of the kernel given by equation (2.24) has been used. The matrix W of the weighting function has the elements $W_{nn} = \nu$ and $W_{nn-1} = W_{n-1n} = n/\sqrt{4n^2 - 1}$.

In order to solve the generalized eigenvalue problem of equation (4.27) one may proceed by inverting either the matrix W or the matrix S, so reducing the equation to a standard eigenvalue problem. However, the matrix W, although symmetric and tridiagonal, may be singular, depending on its order $(N + 1)$ and on the value of ν. This is the case, for example, when $N = 1$ and $\nu = 1/\sqrt{3}$. Fortunately, it is always possible to invert S, either directly, or after eliminating the row and column with $m = 0$ and $n = 0$. This can be deduced from a simple physical argument: consider the *time-dependent*, spatially homogeneous transport equation for a stationary fluid (*cf.* equation (2.6))

$$\Gamma \frac{\partial f}{\partial t} = C(f). \tag{4.30}$$

Separating the variables t and μ (contained in C) leads to the *standard* eigenvalue problem for the matrix $-S$. The time dependence of the solution is

determined by the eigenvalues of S. According to the H-theorem, which applies to both the Fokker-Planck type of collision operator (of which pitch-angle diffusion is a special case) and to the Boltzmann collision operator (of which large-angle scattering is a special case), all distributions evolve towards a unique equilibrium state. In the present case the equilibrium state is that of isotropy, provided absorption is absent. In the presence of absorption, all particles should disappear eventually $f \to 0$ as $t \to \infty$. Therefore, all eigenvalues of S must be positive, except for a possible eigenvalue of zero corresponding to an isotropic eigenfunction. Once this eigenfunction is removed, the resulting matrix is positive definite.

The mathematical proof of the positive definite nature of S, or its reduced version, is straightforward: Since S is a real symmetric matrix, there exists a real orthogonal matrix R, whose columns consist of the eigenvectors of S, such that

$$\sum_{j,k} R_{ji} S_{jk} R_{kl} = \xi_i \delta_{il},$$

where ξ_i are the eigenvalues of S. Now, from the definition of S,

$$\begin{aligned} \xi_i \delta_{i,l} &= \sum_{j,k} \int_{-1}^{+1} \mathrm{d}\mu D_{\mu\mu} \left[R_{ji} \frac{\mathrm{d}P_j(\mu)}{\mathrm{d}\mu} \right] \left[R_{kl} \frac{\mathrm{d}P_k(\mu)}{\mathrm{d}\mu} \right] + \\ &\quad + \sum_{j,k} R_{ji}\, \delta_{jk} (1 - \omega g^j)\, R_{kl}. \end{aligned}$$

Therefore,

$$\begin{aligned} \xi_i &= \int_{-1}^{+1} \mathrm{d}\mu D_{\mu\mu} \left[\sum_j R_{j,i} \frac{\mathrm{d}P_j(\mu)}{\mathrm{d}\mu} \right]^2 + \sum_j (R_{ji})^2 (1 - \omega g^j) \\ &\geq 0, \end{aligned}$$

since $D_{\mu\mu} \geq 0$, for $-1 \leq \mu \leq +1$ and the second term is also ≥ 0 for all $\omega \leq 1$ and $g \leq 1$. Therefore, all the eigenvalues of S are positive, with the possible exception of an isotropic eigenfunction, which would cause the first column of

the orthogonal matrix to read $R_{i0} = \delta_{i0}$. The corresponding eigenvalue is then zero for $\omega = 1$.

In the presence of absorption, therefore, equation (4.27) can be converted directly into a standard eigenvalue problem by inverting S:

$$\sum_{n=0}^{N}\sum_{l=0}^{N}\left(S^{-1}\right)_{ml} W_{ln} q_{ni}^{\nu} = -\frac{1}{\Lambda_i} q_{mi}^{\nu} \qquad [m = 0, \ldots N], \tag{4.31}$$

The $N+1$ eigenvalues and eigenvectors are then found by standard numerical methods [106].

If there is no absorption ($\omega = 1$), the eigenvalue $\Lambda_0 = 0$ must first be removed from the problem. Since the eigenfunction is known to be isotropic, the values of the expansion coefficients q_{n0}^{ν} are easily calculated. With the normalization $Q_0^{\nu}(\mu) = 1/\sqrt{2}$, one finds $q_{00}^{\nu} = 1$. For this eigenfunction to be orthogonal to all the others, the zeroth components of the remaining eigenfunctions must fulfil the condition:

$$q_{0i}^{\nu} = \frac{-1}{\nu\sqrt{3}} q_{1i}^{\nu} \qquad [i = 1, \ldots N]. \tag{4.32}$$

Removing the equation $i = 0$ from the set of equations (4.27) then leads to

$$\sum_{n=1}^{N}\left(W_{mn} - \frac{1}{3\nu}\delta_{n1}\delta_{m1}\right) q_{ni}^{\nu} = -\frac{1}{\Lambda_i}\sum_{n=1}^{N} S_{mn} q_{ni}^{\nu} \qquad [i \neq 0,\ m = 1, \ldots N], \tag{4.33}$$

where the matrix S_{mn}, $[m, n = 1, \ldots N]$, is positive definite. After inversion, one again obtains a standard eigenvalue problem similar to equation (4.31), but with the order reduced by one.

4.2.1 Pitch-Angle Diffusion

Figures 4.2 and 4.3 present results obtained using the methods described above for the case of isotropic pitch-angle diffusion in the absence of absorption: $\nu_\ell = 0$, $\omega = 1$, $\hat{D}_{\mu\mu} = 1 - \mu^2$. The matrix S is in this case diagonal, with elements $S_{nn} = n(n+1)$, and its inversion presents no difficulty.

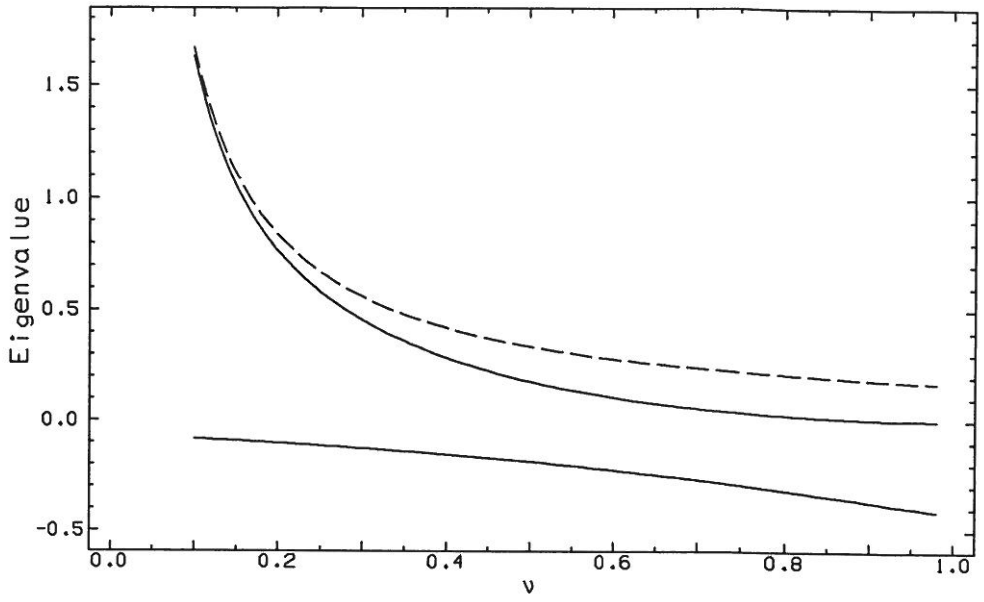

Figure 4.2: The largest and smallest eigenvalues λ_1 and λ_{-1} defined by equation (4.35), for the case of isotropic pitch-angle diffusion, as a function of the ratio of the fluid velocity to the particle velocity. The approximation for λ_1 from diffusion theory is shown as the dashed line.

The eigenvalues are ordered according to the prescription $\Lambda_i < \Lambda_{i+1}$ for both positive and negative i, as well as the special case $\Lambda_0 = 0$. These eigenvalues determine the spatial dependence of the component of the distribution attributed to the associated eigenfunction. Thus, the "range" R of an eigenfunction may be defined as its e–folding length in space, and is given from equation (4.1) by

$$R = |\Gamma v/\Lambda_i|. \tag{4.34}$$

A convenient quantity, proportional to the range, is defined, by analogy with equation (4.9), as

$$\lambda_i \equiv \nu_s/\Lambda_i. \tag{4.35}$$

The largest and smallest λ_i correspond to the eigenfunctions with largest range which are permitted in the upstream and downstream regions, respectively and are shown in Figure 4.2. At particle speeds large compared to the fluid speed

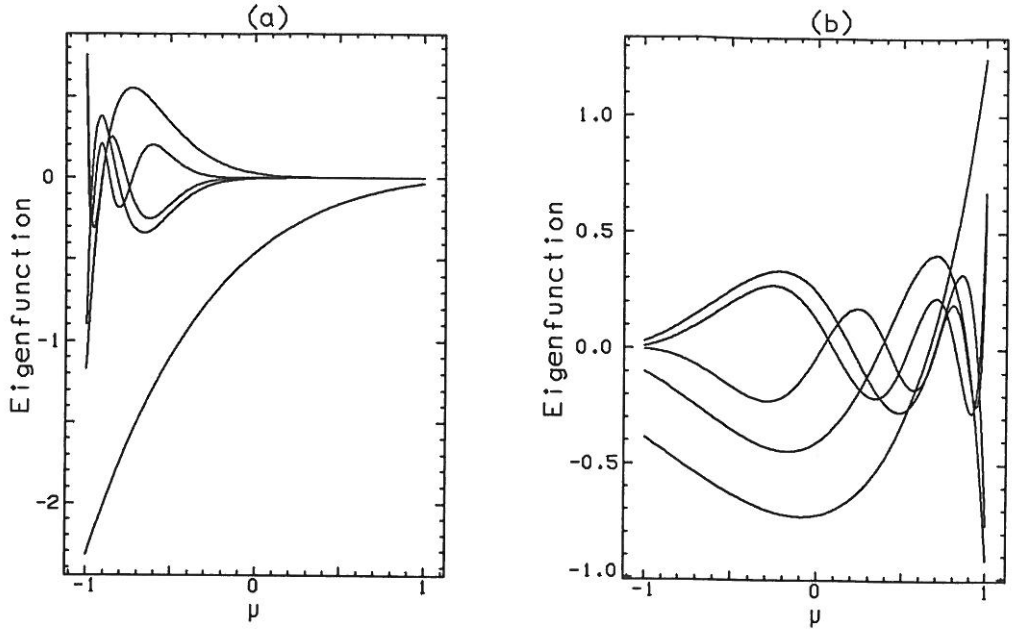

Figure 4.3: The eigenfunctions $Q_i^\nu(\mu)$ for $i = 1 \ldots 5$ (a) and for $i = -1 \ldots -5$ (b). Those of (a) correspond to positive eigenvalues, and may be used to represent the distribution in the upstream region, whereas those of (b) have negative eigenvalues, and are permitted components of downstream distributions.

($\nu << 1$), the approximation from diffusion theory, equation (4.24), which is simply $\lambda_1 = (6\nu)^{-1}$ in this case, is accurate. At speeds approaching that of the fluid, but still larger than it, the largest eigenvalue tends to zero, reflecting the small range of such particles into the upstream region.

The eigenfunction corresponding to λ_1 of Figure 4.2 is shown in Figure 4.3a for $\nu = 1/2$, together with four eigenfunctions of shorter range: Q_2^ν - Q_5^ν. Note that $Q_1^\nu(\mu)$ is the only eigenfunction with no root in the range $-1 \leq \mu \leq +1$. The others possess $i - 1$ roots, and vary more rapidly as their range decreases. The oscillations occur for $-1 < \mu < -\nu$. As one may readily show from equation (4.2), the eigenfunctions may have neither a root nor a turning point for $-\nu < \mu < 1$. The corresponding five eigenfunctions of negative eigenvalue are shown in Figure 4.3b. In this case, the number of roots is $|i|$, and the oscillatory behaviour occurs in the interval $-\nu < \mu < 1$.

Because this is a larger interval than in Figure 4.3a, these functions are easier to represent as a sum of Legendre polynomials (20 of which are used here).

Turning to pitch-angle diffusion with the diffusion coefficients depicted in Figure 2.1, the problem arises of evaluating the elements of the matrix S. A rapid numerical solution can be found by evaluating the integrals in equation (4.28) using Gauss-Legendre quadrature. It is helpful to note that the evaluation of the weights automatically provides the derivatives of the P_n [81]. The generalized eigenvalue problem (similar to equation 4.27) must then be converted into a standard problem. However, instead of inverting S, it is numerically more economical to use standard routines (e.g. from the "NAG–library") to perform a factorization of S into the product of a lower-triangular matrix and an upper-triangular one. The remaining steps are straightforward; details of the method may be found in the monograph by Wilkinson [106]. Results of this procedure are shown in Figures 4.4 and 4.5, where the parameter q, which is connected with the spectrum of the Alfvén turbulence (equation 2.8), has been set equal to 2 in order to enhance the effect of the "dip" in the diffusion coefficient around $\mu = 0$. Figure 4.4 shows the ratio of the range — from equation (4.34) — of the eigenfunction Q_1^ν, which determines the length of the precursor to a shock front, to the value for this quantity given by the diffusion approximation (equations 4.24 and 4.35). Three values of the parameter ϵ have been chosen: $\epsilon = 1/30$, $1/10$ and $1/3$. It can be seen that the value of ϵ has some effect on the range of the eigenfunction Q_1^ν i.e. of the precursor to the shock front. The difference between $\epsilon = 1/30$ and $\epsilon = 1/3$ reaches a factor of 2 at $u/v = 0.6$, with the larger value of ϵ having the longer range (relative to the value in the diffusion approximation). The reduction over the values given by the diffusion approximation is also striking — roughly

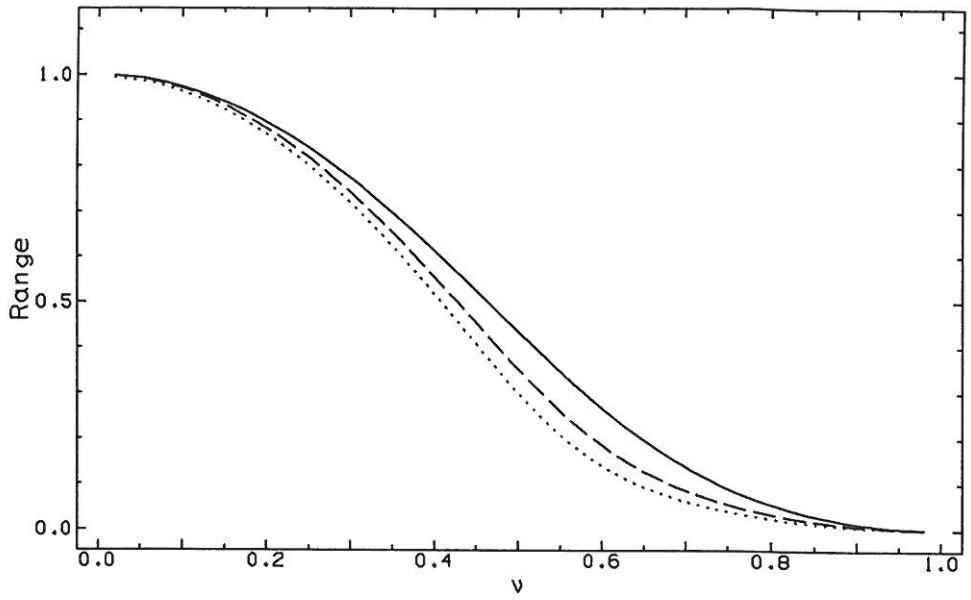

Figure 4.4: The length of the precursor to a shock, normalized to the value given by the diffusion approximation, as a function of the ratio of the speed of the upstream plasma to the particle velocity. The spectral index of the Alfvén turbulence is $q = 2$ and the values $\epsilon = 1/30$ (dotted line), $\epsilon = 1/10$ (dashed line) and $\epsilon = 1/3$ (solid line) are shown.

a factor three for particles moving twice as fast as the shock $u/v = 1/2$.

This figure also indicates the accuracy of the Galerkin method. For the smallest value of ϵ, many Legendre polynomials are needed to deal with the quickly changing value of the diffusion coefficient at $\mu = 0$. In the calculations shown, 50 polynomials were used, with a 200 point Gauss-Legendre quadrature employed to evaluate the matrix S. Since the curves in Figure 4.4 are normalized using the exact value of the precursor length in the diffusion approximation, they must tend to unity as $u/v \to 0$. An error of about 0.5% is visible for $\epsilon = 1/30$. For smaller values of ϵ it would probably be preferable to integrate the differential equation (4.2) directly to find the eigenvalues, rather than use the Galerkin method.

The eigenfunctions corresponding to the eigenvalues of Figure 4.4 are

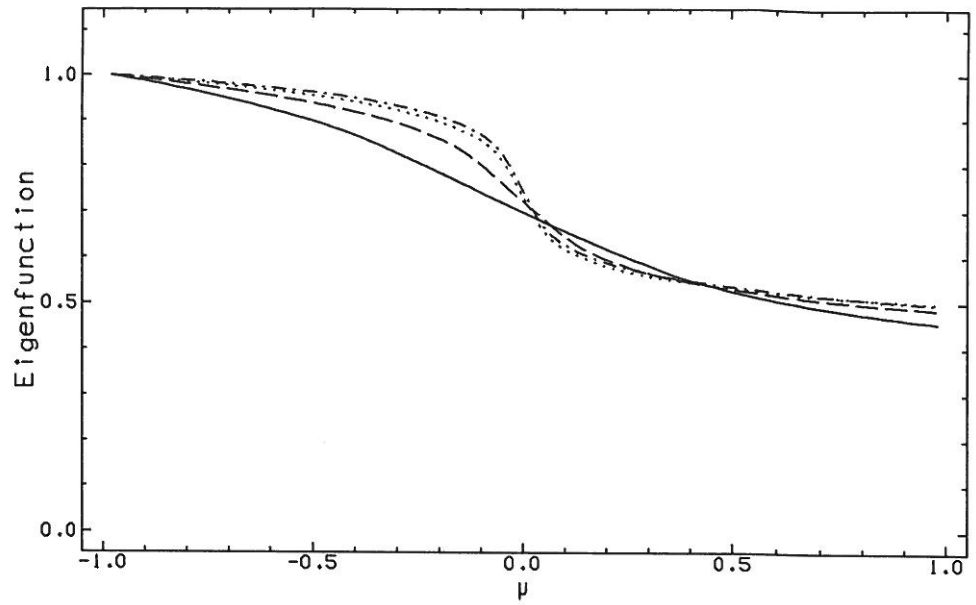

Figure 4.5: The eigenfunctions corresponding to the eigenvalues of Figure 4.4 ($q = 2$ with $\epsilon = 1/30$ (dotted line), $\epsilon = 1/10$ (dashed line) and $\epsilon = 1/3$ (solid line)) for the ratio of the fluid velocity to the particle velocity $\nu = .15$. Also shown is the result of the diffusion approximation (dot–dashed line) for $\epsilon = 1/30$.

shown in Figure 4.5 for $\nu = .15$ and Figure 4.6 for $\nu = 1/2$. The results of the diffusion approximation are shown only for the lower value of ν. Already at $\nu = 1/2$, the diffusion approximation yields an unphysical eigenfunction which contains a root in the interval $-1 \leq \mu \leq 1$. The most prominent feature of these figures is the sharp change of the eigenfunction around $\mu = 0$, where the pitch-angle diffusion coefficient is small. This sharp change in the monotonic eigenfunction is most prominent for $\epsilon = 1/30$, as is to be expected.

The ratio of the number of particles moving in the direction $\mu = 1$ (towards the shock) to the number moving in the direction $\mu = -1$ (away from the shock) is more than 50 in Figure 4.6. Even when the diffusion approximation is a valid, such as in Figure 4.5, this number — now 2 — reflects a relatively strong anisotropy.

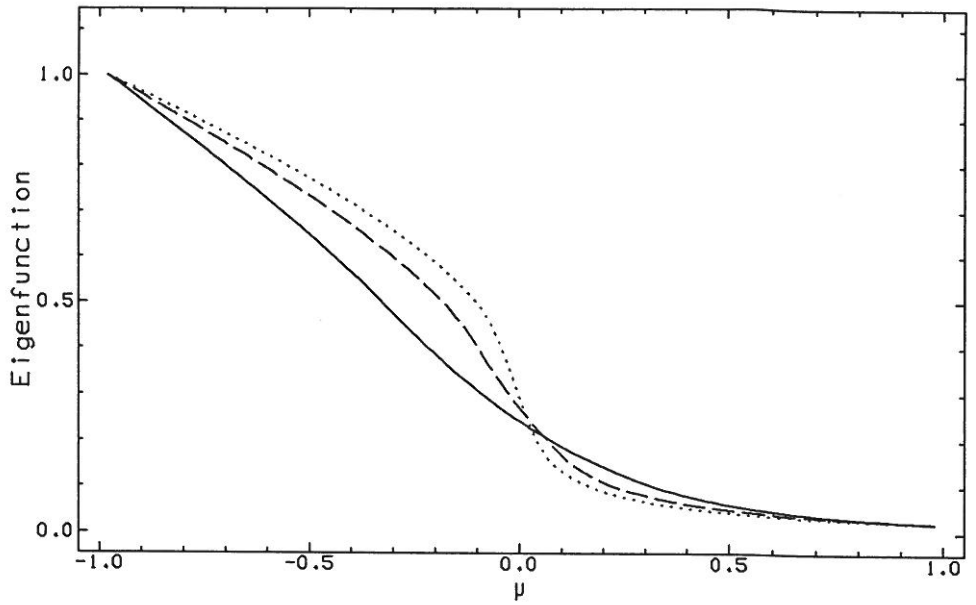

Figure 4.6: The eigenfunctions corresponding to the eigenvalues of Figure 4.4 ($q = 2$ with $\epsilon = 1/30$ (dotted line), $\epsilon = 1/10$ (dashed line) and $\epsilon = 1/3$ (solid line)) for the ratio of the fluid velocity to the particle velocity $\nu = .5$.

4.2.2 Mixed Operator

The Galerkin method yields N approximations to the eigenvalues and eigenfunctions when the highest order Legendre polynomial used in the expansion is P_N. When the mixed operator is used, the values of the largest and smallest eigenvalues $\lambda_{\pm 1}$ quickly stabilize, as N is increased. This is followed by the stabilization of $\lambda_{\pm 2}$, and so on. Thus, it is easy to find the number of polynomials required in order to determine a particular eigenvalue to a certain desired accuracy. Furthermore, one may conclude that the eigenvalues found in this way belong to the discrete spectrum. In contrast, application of the same method in the absence of pitch-angle diffusion leads to a stabilization of the approximations only for $i = 1$ (when $g = 0$). All other values continue to approach each other as N is increased.

To combine the large and small-angle scattering operators in a mean-

ingful way requires a measure of their relative strength. The approximation discussed, for example, by Case and Zweifel [15] in which the distribution is written as a constant plus a term proportional to μ provides a convenient method, since the resulting spatial diffusion coefficient κ depends only on σ_1 of equation (2.16) for the large-angle operator:

$$\kappa_\ell = \frac{v^2}{3}\frac{1}{\nu_\ell(1-2\sigma_1)}. \tag{4.36}$$

Similarly, for the pitch-angle diffusion operator

$$\kappa_s = \frac{v^2}{6}\frac{1}{\nu_s}. \tag{4.37}$$

Defining an effective diffusion coefficient for the combined scattering operator by $\kappa^{-1} = \kappa_s^{-1} + \kappa_\ell^{-1}$, one finds

$$\left(\frac{df}{dt}\right)_{\text{collisions}} = \frac{v^2}{6\kappa}\left[(1-\beta)C_s + \frac{2\beta}{(1-g)}C_\ell\right] f \tag{4.38}$$

where $\beta = \kappa/\kappa_\ell$ measures the relative contribution of large-angle scattering.

It is interesting to see how the discrete eigenvalues evolve as a function of β. In the limit $\beta \to 1$, it is known that only one positive discrete eigenvalue remains, the remainder forming part of the continuum. Figure 4.7 displays the six largest eigenvalues as a function of β, for $\nu = 0.1$, $g = 0$ (isotropic large-angle scattering) and $\omega = 1$ (no absorption). The largest eigenvalue is only weakly dependent on β. This is, in fact, a result of the manner in which the two scattering operators have been combined. The largest eigenvalue is closely related to the spatial diffusion coefficient through equation (4.25), so that the fact that Λ_1 is almost independent of β merely indicates that at the relatively low value of ν used in Figure 4.7, the simple expansion $f \propto a_0 P_0 + a_1 P_1$ is quite accurate. The other eigenvalues, however, all increase with β and have the limiting behaviour $\lambda_i \to (1-\nu)/2 = 0.45$ for $i \geq 2$, which corresponds

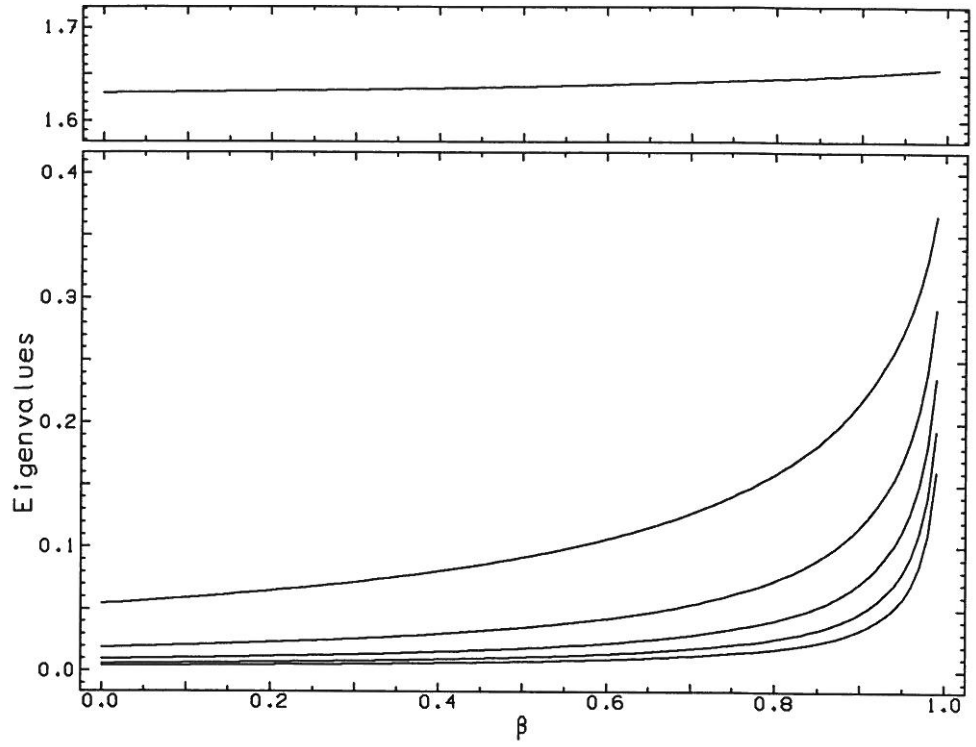

Figure 4.7: The eigenvalues of the combined pitch-angle diffusion and large-angle scattering operator as a function of the relative amount of large-angle scattering β. The six largest eigenvalues are plotted for $\nu = 0.1$ and $g = 0$. Of these, the largest is well separated from the others and is plotted on a separate scale. The remaining five tend towards the end point of the continuum spectrum as $\beta \to 1$.

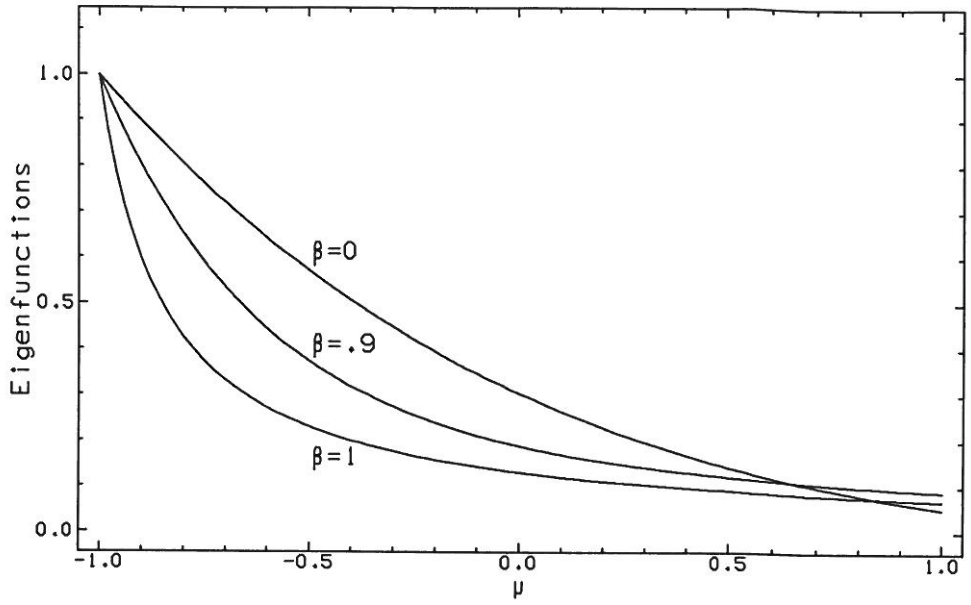

Figure 4.8: The eigenfunctions of largest eigenvalue, for $\nu = 0.4$, and various values of the parameter β, which controls the amount of large-angle scattering in the collision operator. The cosine of the mean scattering angle is $g = 0$.

precisely to the upper end point of the continuum spectrum of the large-angle operator.

To complete the picture, the eigenfunction Q_1^ν corresponding to the largest eigenvalue λ_1 is shown in Figure 4.8. As in the case of pitch-angle diffusion, this eigenfunction is a monotonic function of μ, and does not possess a root within the physically meaningful range $-1 \leq \mu \leq 1$. The effect of increasing the relative amount of large-angle scattering (with $g = 0$ in this case) is to increase the peaking of the function towards $\mu = -1$.

4.3 Solution of the Transport Equation with $f \propto p^{-s}$

4.3.1 Boundary Conditions

Having found the eigenfunctions and eigenvalues and, therefore, the general solution in the form of the expansion (4.1), it remains to impose the boundary conditions and match the upstream and downstream solutions at

the shock front, assuming the accelerated particles to be ultrarelativistic ($v = 1$). Far downstream, the solution is bounded provided the coefficients of all eigenfunctions which correspond to positive eigenvalues vanish; the distribution is driven to isotropy in this limit and is represented solely by the eigenfunction Q_0^ν. Far upstream, the solution is bounded only if there is no component of an eigenfunction of negative eigenvalue. Thus, there are two choices for an upstream boundary condition: either the distribution tends to zero for $z \to -\infty$, i.e. there are no particles in the fluid far upstream, or the distribution tends to a finite isotropic one far upstream, corresponding to an advection of particles into the system by the upstream fluid. (The amplitude of the upstream distribution is arbitrary, since the problem is homogeneous.)

The solutions to be sought are assumed to have everywhere a power-law dependence on momentum p. If particles are advected into the system from far upstream, then these too must have the same power-law index. Physically, a power-law solution cannot apply at all momenta, since the number density of test particles,

$$n = \int_0^\infty dp\, p^2 f, \tag{4.39}$$

would diverge either at the high momentum end of the integration (for $s < 3$) or at the low momentum end (for $s > 3$). Introduction of a cut-off at low momentum p_0 removes this problem, because all solutions are found to have $s > 3$, but an additional boundary condition must be imposed at p_0. However, if the power-law solution is regarded as an approximation which is to apply only at momenta which are large compared to p_0, then one is free to assume that particles with momentum around p_0 are advected into the system with the fluid, or are injected by a source term at any point in the flow. The resulting solution is independent of which of these possibilities actually occurs

and of the boundary condition itself (to within a multiplicative constant). This kind of approximation is not required in the diffusive theory of particle acceleration at shocks, the reason being that the distribution function is known to be isotropic in the downstream region in this theory [22]. Thus, particles may be injected isotropically at momentum p_0 anywhere in the downstream region. On crossing the shock, they undergo only acceleration and never deceleration so that the power-law solution establishes itself for all $p > p_0$, whereas there are no particles with $p < p_0$. In the relativistic case, in which the distribution is not isotropic, several crossings of the shock front may be required before the injected particles "forget" the details of their injection, and assume the angular distribution of the power-law solution, which is attained only for $p >> p_0$.

The power-law assumption also introduces another problem. For all solutions with $f \propto p^{-s}$ and $s \leq 4$, the pressure of the gas of accelerated particles diverges. This problem does not manifest itself in the equations themselves, because the test-particle approach has been adopted. However, it means that the solutions are physically realistic only up to a cut-off momentum, above which an unspecified saturation mechanism is postulated. Various possibilities for this mechanism have been considered in the application to particle acceleration in active galactic nuclei [94]. The problem is not peculiar to relativistic shocks; it arises also in the diffusive theory for shocks of compression ratio greater than 4.

4.3.2 Matching Conditions

The distribution function of accelerated particles (which is a Lorentz scalar) is assumed to be continuous across the shock front. Denoting the upstream momentum and cosine of the pitch-angle by (p, μ) and the downstream

values by $(\tilde{p},\tilde{\mu})$, this matching condition reads:

$$f(p,\mu) \;=\; f(\tilde{p},\tilde{\mu}). \tag{4.40}$$

The relation between (p,μ) and $(\tilde{p},\tilde{\mu})$ is provided by a Lorentz transformation:

$$\tilde{p} \;=\; \Gamma_r p(1+u_r\mu) \tag{4.41}$$

$$\tilde{\mu} \;=\; \frac{\mu+u_r}{1+u_r\mu}, \tag{4.42}$$

where $\Gamma_r = 1/\sqrt{1-u_r^2}$ and u_r denotes the relative velocity of the upstream fluid with respect to the downstream fluid:

$$u_r = \frac{u_- - u_+}{1-u_-u_+}. \tag{4.43}$$

Equation (4.40) cannot, of course, be satisfied exactly if the distribution is represented by only a finite number of eigenfunctions, so that one must have recourse to approximate methods. In the Q_J method [49], one satisfies the boundary conditions downstream and the matching condition at the shock exactly, and attempts to satisfy the boundary conditions upstream approximately. To this end, the distribution function downstream is written:

$$f(\tilde{p},\tilde{\mu},z) \;=\; \tilde{p}^{-s}\sum_{i=-J}^{0}\tilde{a}_i Q_i^{u+}(\tilde{\mu})\exp(\Lambda_i z/\Gamma_+), \tag{4.44}$$

where the $\tilde{a}_i$ are constants and $\Gamma_+ = 1/\sqrt{1-u_+^2}$. This expression satisfies the downstream boundary conditions exactly. According to the matching condition, equation (4.40), the upstream distribution at the shock front, $z=0$, may be computed from equation (4.44) by substituting for $\tilde{p}$ and $\tilde{\mu}$ using equations (4.41) and (4.42). One must now try to fit the upstream boundary conditions as well as possible using the $J+1$ constants $\tilde{a}_i$ and the power-law index s. Although f of equation (4.44) cannot be required to be orthogonal to *all* the upstream eigenfunctions which cause divergent behaviour at $z\to-\infty$,

it can at least be made orthogonal to those J of them with the longest range. Projecting onto the upstream eigenfunctions gives:

$$\Gamma_r^{-s} \sum_{j=-J}^{0} \int_{-1}^{+1} d\mu \, Q_i^{u-}(\mu)(u_- + \mu)(1 + u_r\mu)^{-s} Q_j^{u+}(\tilde{\mu}) \, \tilde{a}_j \;=\; a_i, \quad (4.45)$$

where the a_i are the expansion coefficients of the upstream eigenfunctions $Q_i^{u-}(\mu)$. The boundary conditions thus require $a_i = 0$, for $i < 0$; for a_0, one is free to choose the value 0, for the case in which no particles are advected into the system, or any finite value (e.g. 1), for the case in which a power-law distribution is allowed to enter far upstream. In the former case, the set of $J + 1$ equations (4.45) is homogeneous. The condition that it possess a nontrivial solution is sufficient to determine the unknown power-law index s. In the latter case, the set (4.45) is inhomogeneous. Specification of the power-law index of injected particles enables the downstream distribution (the $\tilde{a}_i$) to be evaluated, provided the specified index is smaller than the value of s found from the homogeneous problem [51].

The numerical procedure for evaluating the determinant of the left-hand side of equation (4.45) is simple. The eigenfunctions are first found in terms of the expansion coefficients of the Galerkin method. Then, the value of each eigenfunction is stored on a grid in μ, together with the quantities $u_- + \mu$ and $1 + \mu u_r$. Finally, the integration is performed over this grid using a trial value of s, and the determinant evaluated. There are, of course, more elegant ways of evaluating the determinant. For example, one can write equation (4.45) entirely in terms of the matrix elements

$$\int_{-1}^{+1} d\mu \, P_m(\mu)(u_- + \mu)(1 + u_r\mu)^{-s} P_n(\tilde{\mu}).$$

A recursion formula can then be derived which enables all elements to be evaluated starting from only the four with $m, n = 0, 1$ — which can themselves

easily be evaluated analytically. This procedure, however, turns out to be fraught with numerical problems arising from the large number of Legendre polynomials (up to 100) necessary to represent the eigenfunctions.

The symmetry of the problem suggests another approach to finding an approximate solution: first fit the upstream boundary conditions exactly, impose the matching condition, and then attempt to fit the downstream boundary conditions by projecting the distribution onto the first J "forbidden" eigenfunctions downstream. A glance at Figure 4.3a,b shows why this method is unsuitable. The eigenfunctions which are forbidden downstream have positive eigenvalues and are shown in (a). They have much more rapid oscillations than the eigenfunctions which are forbidden upstream (b). Therefore, a method which uses only eigenfunctions of positive eigenvalue requires more Legendre polynomials than one which uses only eigenfunctions of negative eigenvalue. The accuracy attainable numerically would be reduced as a result.

CHAPTER V

Results

5.1 A Parameter Survey

Two basically different physical processes influence the spectrum of ultrarelativistic particles accelerated by the first-order Fermi mechanism operating at a parallel, unmodified, relativistic shock front — assuming there are no pre-accelerated particles advected into the system. These are the process responsible for the formation of the collisionless shock front itself, which determines the jump conditions as discussed in §3.2, and the process which gives rise to the collision operator describing the transport of ultrarelativistic particles (§II). Five different possibilities for the jump conditions may be relevant; their effects are investigated below. In the case of the collision operator, the number of possibilities is even larger. However, an overview of the effects at play may be obtained by first restricting consideration to pitch-angle diffusion, as described by two parameters: q, which is related in the quasi-linear theory to the spectrum of Alfvén turbulence, and ϵ, which models the extent to which nonlinear effects enhance the scattering of particles moving almost perpendicular to the magnetic field. Each of these parameters is discussed in §2.2.

Large-angle scattering has a substantial effect on particle acceleration, but there is no theory of turbulence which is capable of predicting a phase-function suitable for modelling the process. In view of this, the investigations

presented here are restricted to isotropic scattering, and emphasize the changes to be expected in the spectrum of particles accelerated by one particular shock when various amounts of large-angle scattering are introduced in the upstream and downstream regions.

5.1.1 Pitch-Angle Diffusion

Consider first the case in which the gas behind the shock front reaches full thermodynamic equilibrium. Using the appropriate jump conditions and assuming that pitch-angle diffusion controls the particles transport, the results of applying the Q_J method are shown in Figure 5.1. In (a), the pitch-angle diffusion coefficient is taken to be isotropic. The scattering matrix S given by equation (4.28) is then diagonal. This case arises whenever the spectrum of Alfvén turbulence is given by $q = 1$, independent of the value of the parameter ϵ. In (b), a highly anisotropic diffusion coefficient is assumed, similar to that shown in Figure 2.1, but with $q = 2$ and $\epsilon = 1/30$. This represents the most anisotropic form of the diffusion coefficient which can be comfortably treated by the methods of §IV. Already it is difficult to extend the range of investigation to very high upstream velocities. In (a), the maximum value is $u_- = .98$, but in (b), satisfactory convergence is obtained only up to $u_- = .9$. As well as the fully converged result of the Q_J method, Figure 5.1 also displays the result of applying the formula $s = 3r/(r-1)$ (with r the compression ratio), which is obtained in the nonrelativistic diffusion theory.

As expected the two curves agree for small upstream speeds. The compression ratio tends to 4 in this case, and s also tends to this limit for small u_-. However, the softening of the equation of state due to the relativistic speed of the thermal electrons quickly makes itself felt as u_- rises. At $u_- = .1$, the power-law index is much harder: $s = 3.7$. The Q_J method and the

nonrelativistic diffusion approximation still agree well at this low value of u_-, indicating that the distribution function of accelerated particles is close to being isotropic. As u_- rises further, the nonrelativistic diffusion approximation predicts a spectrum which is steeper than the "exact" one in both the isotropic case (a) and the anisotropic case (b). A similar result has been obtained by Kirk and Schneider [49] using a fixed compression ratio and an isotropic diffusion coefficient. The discrepancy is, however, not due to the failure of the diffusion approximation, but to the failure of the *nonrelativistic* version of it. A relativistic diffusion approximation can be formulated by assuming isotropy in only the downstream fluid frame. It does not, however, yield a simple expression for the power-law index s [49].

In Figure 5.1a, the exact result remains harder (smaller s) than the value given by the diffusion approximation as u_- is increased towards unity. Both values increase, however, and exceed 4 before u_- reaches the maximum investigated speed of $.98c$. On the other hand, Figure 5.1b shows the effect of the anisotropic diffusion coefficient. The difficulty experienced by particles in crossing over the region $\mu = 0$ reduces the probability of their returning to the shock front once they have entered the downstream fluid. This reduction becomes apparent when the distribution function is driven away from isotropy by the high speed of the fluid through the shock. A decreased probability of recrossing implies a steeper spectrum which is seen in Figure 5.1b for $u_- > .3$. At $u_- = .4$, the exact solution crosses that of the nonrelativistic diffusion approximation and proceeds to even higher values of s.

In §III, four other possible jump conditions were investigated for relativistic shocks. The effects of each of these is displayed in Figure 5.2. For a shock front in a relativistic gas with an equation of state given by equa-

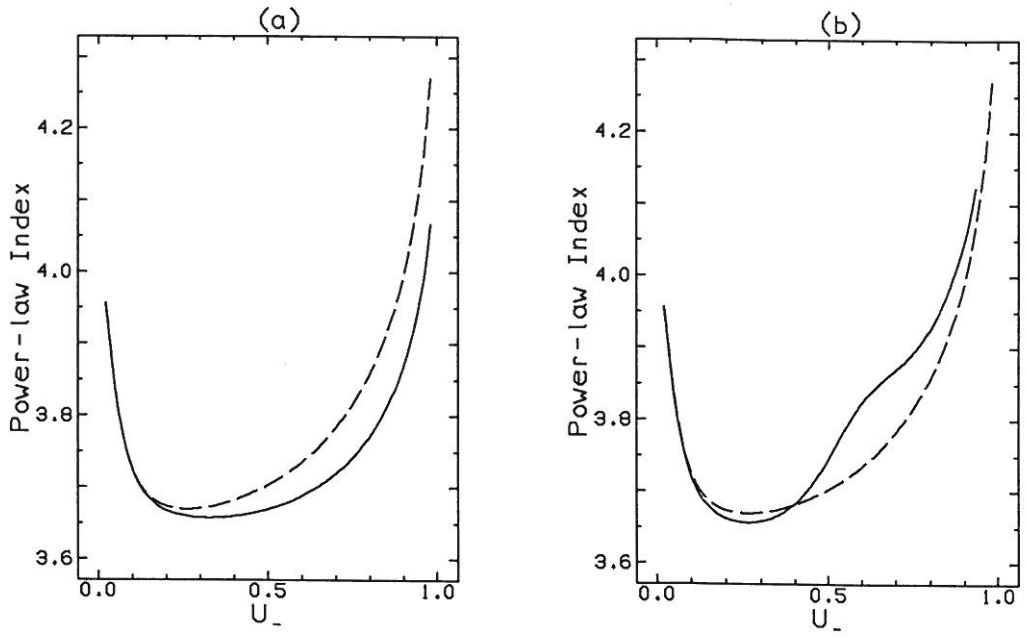

Figure 5.1: The power-law index of particles accelerated by a relativistic shock front when the particle transport is governed by pitch-angle diffusion. In (a), the pitch-angle diffusion coefficient is isotropic, whereas in (b), a highly anisotropic diffusion coefficient with $q = 2$, $\epsilon = 1/30$ is assumed. The jump conditions are for a gas which reaches full thermodynamic equilibrium behind the shock front. The solid curve presents the results of applying the Q_J method; the dashed curve is the result of applying the formula derived from the nonrelativistic diffusion approximation: $s = 3r/(r-1)$ (where r is the compression ratio).

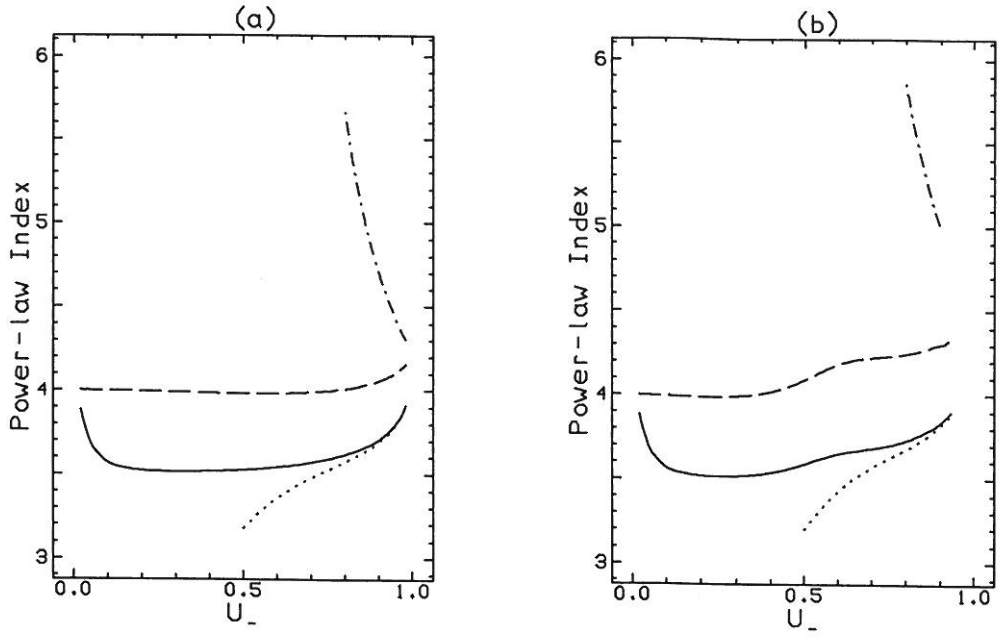

Figure 5.2: The power-law index of particles accelerated by a relativistic shock front when the particle transport is governed by pitch-angle scattering. In (a), the pitch-angle diffusion coefficient is isotropic, whereas in (b), a highly anisotropic diffusion coefficient with $q = 2$, $\epsilon = 1/30$ is assumed. The dash-dotted line corresponds to a relativistic gas with equation of state (3.18). The dashed line is for a strong shock with only ion pressure supporting it, the solid line for support by electron pressure only. The dotted line is for a strong shock with pressure provided by electrons and pairs, the number of these being about 100 per proton [i.e. $\eta = 0.9$ in equation (3.24)].

tion (3.18), the jump conditions are simply $u_- u_+ = 1/3$ (equation 3.40). For $u_- \to 1$, the downstream speed tends to $u_+ = 1/3$, but as the upstream velocity decreases, the downstream velocity *increases* until the shock peters out with $u_- = u_+ = 1/\sqrt{3}$, the sound velocity in an isotropic relativistic gas. Thus, as this shock gets weaker, it advects the downstream particles more quickly away from the region of acceleration. Unlike the other types of shock investigated, this shock is not strong, because the pressure of the upstream gas plays an important role. It is the only case in which the downstream velocity increases as the upstream velocity decreases; as a result, the power-law index of accelerated particles becomes much harder as $u_- \to 1$. Such behaviour can be seen in Figure 5.2b. All other shocks produce a softer spectrum of particles as $u_- \to 1$.

When the pressure behind the shock is provided by the ions alone, the jump conditions remain close to those of a nonrelativistic shock for upstream velocities extending up to about $0.7c$. For isotropic pitch-angle diffusion, the nonrelativistic diffusion approximation provides a reasonably accurate value of s in this range, although a little larger than the exact value, as can be deduced from the discussion of Figure 5.1. However, for the anisotropic case shown in Figure 5.2b, the spectrum steepens markedly at about $u_- = 0.4$, indicating that the particles can no longer be kept isotropic by this relatively ineffective pitch-angle diffusion. A similar, but less pronounced steepening can be observed in the spectrum calculated for the case in which only electron pressure is present behind the shock. The spectrum in this case is generally much harder, because of the softer equation of state which becomes important already at quite low upstream velocities.

Pair-production in the shock front produces a dramatic effect on the spectrum which is rather insensitive to the kind of pitch-angle diffusion as-

sumed. As is pointed out in the discussion of §III, the compression ratio of the shock is greatly increased if some of the energy is channelled into electron–positron pairs. The resulting hard spectrum is shown in Figure 5.2. For $u_- < 0.5$ it approaches the value of 3, corresponding to equal numbers of accelerated particles in each decade of the entire momentum space. This value can be attained only if the probability of a particle escaping to $z = \infty$ in the downstream fluid is zero — i.e. if the downstream fluid is stationary.

5.1.2 Mixed Operator

The number of free parameters available in describing large-angle scattering is even larger than in the case of pitch-angle diffusion. Furthermore, there is no quantitative theoretical basis which could limit the choice significantly. Therefore, in investigating the general effect of such scattering, only the simplest case will be considered. All results of this section refer to a shock with upstream velocity $u_- = .9$ and jump condition $u_+ = (3u_-)^{-1}$. No absorption is permitted ($\omega = 1$), and the scattering operator is a mixture of isotropic pitch-angle diffusion and large-angle scattering described by the Henyey–Greenstein phase function (equation 2.19). The relative amount of large-angle scattering compared to pitch-angle diffusion is given by the parameter β as described in §4.2.2.

In Figures 5.3a, b and c, the behaviour of s for a relativistic shock is depicted. First of all, the case in which the upstream and downstream scattering laws are the same is presented. Figure 5.3a shows s as a function of β $(= \beta_- = \beta_+)$ for various values of g $(= g_- = g_+)$. In this case the spectrum is hardened considerably by increasing the relative contribution of large-angle scattering (increasing β) or by increasing the average scattering

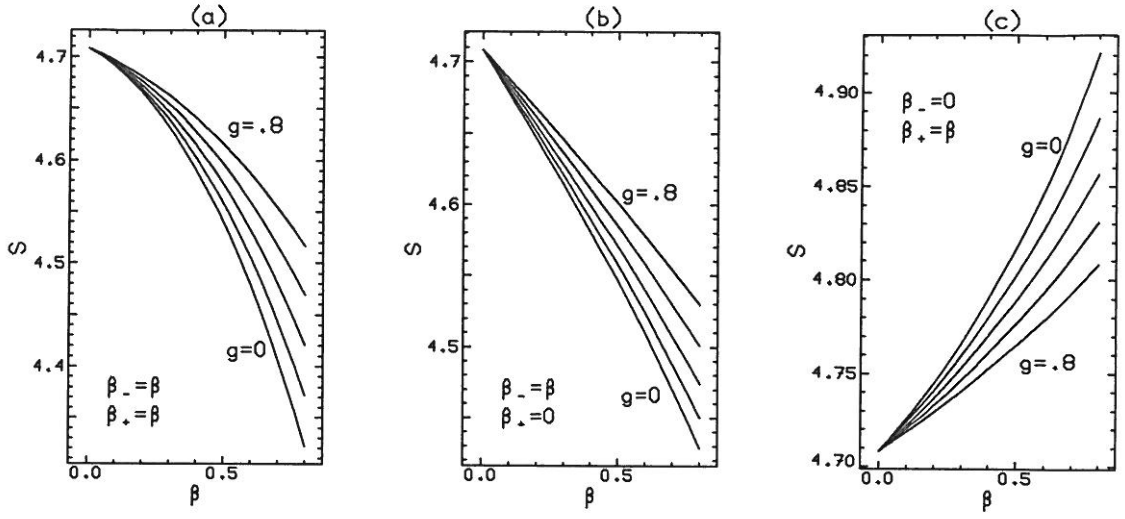

Figure 5.3: The power-law index s for the mixed operator consisting of pitch-angle diffusion and large-angle scattering, without absorption. A relativistic shock is taken, with $u_- = .9$ and $u_+ = 1/3u_-$. In (a), large-angle scattering is permitted both upstream and downstream, in (b) only upstream and in (c) only downstream. The values of the cosine of the mean scattering angle are $g = 0$, .2, .4, .6 and .8. The dependence of s on g is monotonic for each β.

angle (decreasing g). For isotropic scattering, s changes by about 10% when β goes from 0 to 0.8.

The situation becomes more complicated when large-angle scattering is included in only the upstream or only the downstream medium (leaving just pitch-angle diffusion in the other medium). In the first case ($\beta_+ = 0$), which is shown in Figure 5.3b, The effect is similar to that observed in Figure 5.3a, but not quite as strong. However, if large-angle scattering is permitted only downstream (Figure 5.3c), the effect is opposite — the spectrum *softens* with increasing effectiveness of large-angle scattering. To understand these results, it is instructive to consider the process of particle acceleration as a competition between the tendency of a particle to escape from the shock by being advected downstream and the fractional increase in momentum which it gains by making an excursion into the upstream medium. The index s is related to the ratio

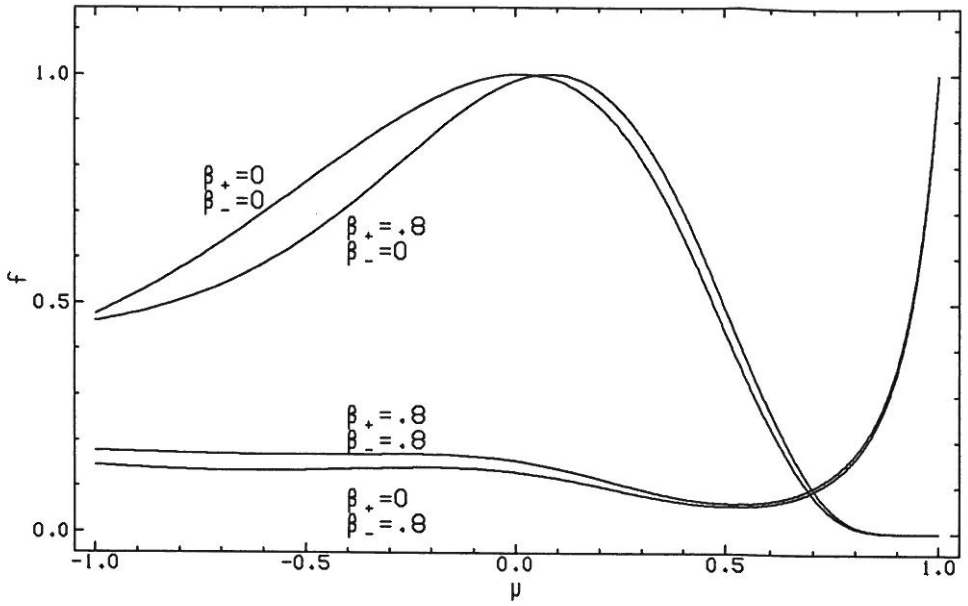

Figure 5.4: The distribution function f at the relativistic shock front of Figure 5.3 as a function of the cosine μ of the pitch-angle measured in the downstream fluid frame for $g = 0$. The effects of switching on and off large-angle scattering in the upstream and downstream regions is displayed.

of these quantities. As a rough guide to interpretation, one can say that the fractional gain in momentum is largely determined by the scattering which occurs during the excursion into the high-speed upstream region. If a particle reenters the downstream region moving close to the shock normal, the gain in momentum is much larger than if it enters moving almost parallel to the shock surface. When only pitch-angle diffusion is included, most particles cross into the downstream region moving almost parallel to the shock surface. This can be seen in Figure 5.4 where the distribution function at the shock is displayed as a function of the cosine of the downstream pitch-angle ($\tilde{\mu}$). When large-angle scattering is introduced upstream, this distribution is changed dramatically. A peak consisting of particles crossing the shock with $\tilde{\mu} \approx 1$ appears, which is easy to understand as consisting primarily of the Lorentz boosted distribution of particles which have suffered a large-angle scattering event upstream. The

fractional energy gain of such particles is large compared to that of those particles which return without suffering a large-angle scattering. Thus, one is able to understand that for a fixed type of downstream scattering, increasing the effectiveness of upstream scattering hardens the spectrum.

The situation is different when the downstream scattering is varied. The fractional momentum gain is not sensitive to the angle at which a particle leaves the downstream region. In fact, in the shock frame, a particle which returns to the shock front from the downstream region has a slightly lower momentum than it had upon entering this region. The change is small because the downstream fluid moves much more slowly relative to the shock front than the upstream fluid. However, changing the downstream scattering law has a marked effect on the escape probability. From Figure 5.4, one sees that particles entering the downstream region have a distribution either peaked parallel to the shock surface ($\beta_- = 0$) or parallel to the shock normal ($\beta_- = 0.8$). Large-angle scattering downstream tends to move particles rapidly out of the peak of the distribution, whereas pitch-angle diffusion tends to broaden the peak. Thus, in the first case, pitch-angle diffusion can be quite effective in sending particles back across the shock, since the peak is already almost parallel to the shock surface. Increasing the relative amount of large-angle scattering inhibits this process by destroying the peak. Thus, when only pitch-angle diffusion is present upstream, increasing the effectiveness of large-angle scattering downstream increases the escape probability and, therefore, softens the spectrum. This effect is seen in Figure 5.3c.

Consider now the case in which the distribution of particles entering the downstream region is peaked along the shock normal, i.e. the case in which large-angle scattering dominates upstream. Pitch-angle scattering

succeeds only in broadening the peak, so that it is ineffective at reversing the direction of motion of particles in the peak of the distribution. Reversal is, however, required in this case, if particles are to return to the shock. Large-angle scattering, on the other hand, is effective at reversing the particle direction. Consequently, increasing the amount of large-angle scattering *reduces* the escape probability when the distribution is peaked along the shock normal. This results in the harder spectra of Figure 5.3a compared to those of Figure 5.3b.

In summary, the introduction of large-angle scattering has a substantial effect on the slope of the spectrum of accelerated particles. If it dominates only upstream, the spectrum is harder than in the case of pure pitch-angle diffusion. If it dominates only downstream, the spectrum is softer. If both upstream and downstream are dominated by large-angle scattering, the hardest spectral index of all is obtained.

5.2 An Astrophysical Application

Fluid motions at speeds approaching the velocity of light are implied in the nuclei of active galaxies and quasars for two reasons. Firstly, the proper motion of distinct "knots" or "components" has been observed in small-scale jets emerging from the cores of such objects [108]. Although the motion is small (of the order of 10^{-3} arcseconds per year), when combined with the large distance obtained from the standard cosmological interpretation of the observed redshift, the apparent speed projected onto the plane of the sky frequently lies in the range 1–10 times c. The most plausible explanation of this phenomenon is that one is observing the apparent velocity of a source moving at a speed close to c in a direction almost directly at the observer [83,90]. Relativistic speeds are also implied by the fact that the so-called "Compton Catastrophe"

apparently does not occur in AGN's and quasars. This phenomenon predicts a very high X-ray flux from any source of synchrotron radiation which has a brightness temperature in the radio greater than about 10^{12}K [44]. Such X-ray fluxes are not observed, although radio brightness temperatures of 10^{15}K are often found in the cores of AGN's and quasars when an estimate of the size of the emitting region is available. Sometimes such an estimate can be made from the timescale over which broad band variations of the radio emission occur [73]; less frequently from a direct measurement of the angular size of the object [64]. Once again, the standard explanation is that the observed brightness temperature is boosted by the Lorentz factor associated with the relativistic motion of the source towards the observer — in the frame of reference in which the source is stationary, however, the brightness temperature does not violate the limit imposed by the Compton Catastrophe. In cases in which the radio flux at high frequencies does not vary rapidly, and in which the object is too small to be resolved, the variability of the low-frequency radio emission has been used to estimate the size of the source [39]. Again, this frequently leads to apparent contradictions with the observed X-ray flux (or upper limit) [19]. However, there is considerable uncertainty involved in interpreting the timescale of variation as the light crossing time of the source. It is probable that such variations arise during the propagation of the signal through the interstellar medium [85], as seems to be the case with pulsars [93].

In view of this evidence, models have been advanced to explain the spectrum of "superluminal" sources in terms of the synchrotron radiation of a distribution of relativistic electrons carried by a relativistically moving jet [83,12,8]. Geometrical factors tend to have a large effect on the predictions of such models and have usually been emphasized at the expense of the physics of

the particle acceleration. However, the results of §5.1.1 are directly applicable to such situations and provide a functional dependence of the power-law index of an accelerated electron distribution on the speed of the shock front.

Consider the model in which the knots of a superluminal jet are produced by a relativistically moving shock front. The direction and speed of the front differ from that of the fluid, so that the knot can move either away from the core of the AGN or towards it [59]. In a few cases, complicated patterns of motion are in fact observed [76]. However, the motion of the knots is usually in the outward direction; presumably in the same direction as the fluid flow. Two different situations are possible: either the shock moves inward relative to the fluid, in which case material closer to the central object is cold, unshocked fluid and the outward velocity of the shock is lower than that of the unshocked fluid, or the shock moves outward relative to the fluid, in which case the outward velocity of the shock is larger than that of the unshocked fluid. Since the shock front is presumably formed as a result of a nonuniformity in the flow, one would expect both kinds of shock to develop at each knot. An obstacle in the flow, such as, for example, a dense gas cloud, would form a shock which moves into the obstacle as well as a reverse shock propagating back into the flow [1]. In practice, one of these shock fronts will be stronger than the other, in the sense that it will tend to accelerate particles into a harder power-law spectrum. Then it is reasonable to suppose that most of the observed radiation comes from particles accelerated by this shock front.

Perhaps the most detailed recent model of a shock front in a relativistic jet is that proposed by Marscher and Gear [65] to account for observations of the flare in the quasar 3C 273 which occurred in 1983. This object was, in fact, the first in which superluminal motion of a component was discovered

[79]. A dramatic increase of the flux at millimeter to micrometer wavelengths was observed [87] in early 1983, which it is attractive to associate with the emergence of a new knot from the core of the radio source [14], similar to events previously detected by VLBI observations. In the model, the knot is assumed to be a shock front propagating away from the core. Observations in the far-infrared are particularly useful, since electrons which radiate in this frequency range have rather short lifetimes (of the order of weeks). Thus, one is looking at electrons close to the shock itself — if that is where the acceleration occurs. The much longer radiative lifetimes of electrons which emit at gigaherz frequencies, on the other hand, mean that the properties of the flow behind the shock front (where the plasma probably undergoes re-expansion) may play a major role in forming the spectrum.

The model proposed in [65] uses a fixed value for the power-law index of radiating electrons which corresponds to $s = 4.4$ for the quiescent component (i.e. the radio emission present before and after the flare) and $s = 5.4$ for the flare itself. These values are obtained by assuming the spectrum in the far-infrared is either optically thin synchrotron radiation, or comptonized radiation; in each case the observed spectral index of radiative energy flux α is related to s by the formula

$$\alpha = \frac{s-3}{2}. \tag{5.1}$$

However, if we assume that the shock front continually accelerates electrons which subsequently cool in the downstream region, the index of the observed power-law spectrum is steeper by 0.5 than the value implied by equation (5.1). This is because the volume occupied by energetic electrons radiating at high frequencies is smaller than the volume occupied by those radiating at low frequencies (which take a longer time to cool after leaving the shock front [72]).

Thus, the model requires a shock front to accelerate electrons into a power-law spectrum with index $s = 4.4$, which subsequently cool to produce the flare spectrum. Figures 5.1 and 5.2 indicate that this value is rather too steep for a strong relativistic shock. If the plasma reaches thermodynamic equilibrium behind the shock, or if electron pressure dominates, a very much lower value of s is predicted ($\lesssim 4$). Only if the jump conditions are such that ion pressure supports the shock, can a reasonable value be obtained ($s = 4.3$ at $u_- = .9$), and this only when the pitch-angle diffusion coefficient is assumed to possess a significant "hole" around $\mu = 0$ (see Figure 5.2b). An interesting alternative to this picture is that of a shock front which is not strong. If, for example, the pressure in both the upstream and downstream regions is dominated by the radiating electrons themselves, the expected value of s is given by the dot-dashed curve in Figure 5.2, corresponding to a relativistic gas. Much higher values of s are then expected, and these increase rapidly as the shock loses strength. Another possibility is that relativistic shocks may not be treated as a discontinuous jump in the fluid velocity. Shocks of finite thickness (compared to the mean free path of the energetic particles) have been found to produce a steepening of the spectrum, at least in the diffusion approximation [13,92].

The above interpretation rests on the assumption that particle transport can be described by the pitch-angle diffusion operator. As yet, it is not known whether or not the large-angle scattering operator introduced in §2.3 is an accurate way of modelling the effects of strong plasma turbulence and this question is much more likely to be addressed by *in situ* observations of particles accelerated at shock fronts in the solar system. In particular, the anisotropy which is produced at the shock front by the inclusion of large-angle scattering is a characteristic feature which is in principle measurable. How-

ever, in the absence of a better guide, the results presented in Figure 5.3 may be interpreted as indicating that the value of s could be changed by as much as 0.4 if such scattering were present. The steeper values of s which seem to be indicated by the above discussion would result if large-angle scattering occurred predominantly in the downstream region.

Flaring behaviour is not confined to the quasar 3C273. In a recent survey of BL Lac objects and optically violent variable quasars (collectively termed Blazers), Gear *et al.* [31] find variability consistent with the interpretation that relativistic jets, possibly containing shock fronts are responsible. Of the 12 sources studied, 5 are known to display superluminal motion. The spectral indices measured for the optically thin emission in the highly variable 1–4μm range imply electron injection with $4 \lesssim s \lesssim 6.4$, indicating a wide variety of shocks. However, none of the observations is compatible with injection at $s < 4$, such as would be expected from a strong shock dominated by electron pressure.

Much of the difficulty of modelling the flaring behaviour of AGN's is associated not with the spectral index, but with the time dependence of the observed flux, a subject not touched upon in the discussion presented above. The time dependence, however, can be discussed in a relatively simple model of the type proposed by Marscher and Gear [65]. On the other hand, older models, which deal with expanding homogeneous plasma clouds, [54,77] generally predict a decrease in time of the peak flux, in contrast to the observed increase. Those models which do not include shock fronts resort to specifying continuous reacceleration of the electrons throughout the emission region (usually an expanding jet) [63,18,100] and encounter problems in explaining the simultaneous variation of the optically thin emission at all frequencies.

Further work is clearly required in order to incorporate into realistic models both the jump conditions for relativistic shocks and — more especially — the dependence of the index s on these conditions. Because the angular dependence of the electron distribution would then be obtained (see Figure 5.4) such a model would be capable of more detailed predictions concerning, for example, the degree of circular polarization to be expected.

Investigations of this kind go beyond the scope of the thesis presented here. However, even a preliminary application shows that it is not difficult to envisage a relativistic shock front capable of accelerating electrons into the required power-law spectrum. On the contrary, since the strong shocks investigated produce harder spectra than those observed, one is faced with the more agreeable problem that the mechanism is, if anything, too effective.

Acknowledgments

Many of the ideas presented in this thesis arose in the course of a continuing collaboration with Dr. P. Schneider. I thank him also for his comments and suggestions concerning the remainder. I further thank Drs. R. Schlickeiser and G. M. Webb for discussions which proved valuable in clarifying several issues addressed herein.

Bibliography

[1] Aller, H. D., Aller, M. F. and Hughes, P. A. 1985 *Astrophys. J.*, **298**, 296.

[2] Arp, H. 1987 *Quasars, Redshifts and Controversies* (Berkeley, California: Interstellar Media).

[3] Axford, W. I. 1980 in *Origin of Cosmic Rays* IAU Symposium No. 94, eds. G. Setti, G. Spada, A. N. Wolfendale, page 339.

[4] Axford, W. I., Leer, E. and Skadron, G. 1977, in *Proceedings of the 15th International Cosmic Ray Conference* Plovdic (Budapest: Central Research Institute for Physics) **11**, 132.

[5] Begelman, M. C., Blandford, R. D. and Rees, M. J. 1984 *Rev. Mod. Phys.* **56**, 255.

[6] Bell, A. R. 1978 *Mon. Not. R. Astr. Soc.*, **182**, 147.

[7] Blandford, R. D. and Eichler, D. 1987 *Phys. Rep.* **154**, 1.

[8] Blandford, R. D. and Königl, A. *Astrophys. J.*, **232**, 34.

[9] Blandford, R. D. and McKee, C. F. 1976 *Phys. Fluids* **19**, 1130.

[10] Blandford, R. D. and Ostriker, J. P. 1978 *Astrophys. J.*, **211**, L29.

[11] Blandford, R. D. and Payne, D. G. 1981 *Mon. Not. R. Astr. Soc.*, **194**, 1041.

[12] Blandford, R. D. and Rees, M. J. 1974 *Mon. Not. R. Astr. Soc.*, **169**, 395.

[13] Bogdan, T. J. and Lerche, I. 1985 *Mon. Not. R. Astr. Soc.*, **212**, 413.

[14] Bregman, J. N. 1986, in *Quasars* IAU Symposium No. 119, eds G. Swarup, V. K. Kapahi (Dordrecht: Reidel), page 65.

[15] Case, K. M. and Zweifel, P. F. 1967 *Linear Transport Theory* (London: Addison-Wesley).

[16] Castor, J. I. 1972 *Astrophys. J.*, **178**, 779.

[17] Chandrasehkar, S. 1960 *Radiative Transfer* (New York: Dover).

[18] Clegg, P. E., Gear, W. K., Ade, P. A. R., Robson, E. I., Smith, M. G., Nolt, I. G., Radostitz, J. V., Glaccum, W., Harper, D. A. and Low, F. J. 1983 *Astrophys. J.*, **273**, 58.

[19] Condon, J. J. and Dennison, B. 1978 *Astrophys. J.*, **224**, 835.

[20] Courant, R. and Hilbert, D. *Methods of Mathematical Physics* (New York: John Wiley).

[21] Davilla, J. M. and Scott, J. S. 1984 *Astrophys. J.*, **285**, 400.

[22] Drury, L. O'C. 1983 *Rep. Prog. Phys.*, **46**, 973.

[23] Duderstadt, J. J. and Martin, W. R. 1979 *Transport Theory* (New York: John Wiley).

[24] Earl, J. A. 1974 *Astrophys. J.*, **188**, 379.

[25] Ehlers, J. 1971, in *General Relativity and Cosmology*, proceedings of course 47, International School of Physics 'Enrico Fermi', §22.6.

[26] Federenko, V. N. 1984 *Sov. Astron.*, **27**, 640.

[27] Fermi, E. 1949 *Phys. Rev.* **75**, 1169, also *Collected Papers vol. II* page 656 (1965 Chicago: University of Chicago Press).

[28] Fermi, E. 1954 *Astrophys. J.*, **119**, 1, also *Collected Papers vol. II* page 970 (1965 Chicago: University of Chicago Press).

[29] Finlayson, B. A. 1972 *The Method of Weighted Residuals and Variational Principles* (New York: Academic Press)

[30] Forman, M. A. and Webb, G. M. 1985, in *Collisionless Shocks in the Heliosphere: A Tutorial Review*, ed. R. G. Stone and B. T. Tsurutani, Geophysical Monograph Series, **34**, 91.

[31] Gear W. K., Brown, L. M. J., Robson, E. I., Ade, P. A. R., Griffin, M. J., Smith, M. G., Nolt, I. G., Radostitz, J. V., Veeder, G. and Lebofsky, L. 1986 *Astrophys. J.*, **304**, 295.

[32] Goldstein, M. L. 1976 *Astrophys. J.*, **204**, 900.

[33] Henyey, L. G. and Greenstein, J. L. 1941 *Astrophys. J.*, **93**, 70.

[34] Holman, G. D., Ionson, J. A. and Scott, J. S. 1979 *Astrophys. J.*, **228**, 576.

[35] Johnson, M. H. and McKee, C. F. 1971 *Phys. Rev.* **D3**, 858.

[36] Jokipii, J. R. 1966 *Astrophys. J.*, **146**, 480.

[37] Jokipii, J. R. submitted to *Astrophys. J.*

[38] Jones, F. C., Kaiser, T. B. and Birmingham, T. J. 1973 *Phys. Rev. Letts.*, **31**, 485.

[39] Jones, T. W. and Burbidge, G. R. 1973 *Astrophys. J.*, **186**, 791.

[40] Kamke, E. 1983 *Differentialgleichingen Lösungsmethoden und Lösungen* (Stuttgart: Teubner).

[41] Kato, T. 1976 *Perturbation Theory for Linear Operators* (New York: Springer).

[42] Kazanas, D. and Ellison, D. C. 1986 *Astrophys. J.*, **304**, 178.

[43] Kazanas, D. and Ellison, D. C. 1986 *Nature* **319**, 380.

[44] Kellermann, K. I. and Pauliny-Toth, I. I. K. 1969 *Astrophys. J.*, **155**, L71.

[45] Kennel, C. F., Coroniti, F. V., Scarf, F. L., Livesey, W. A., Russell, C. T., Smith, E. J, Wenzel, K. P. and Scholer, M. 1986 *J. Geophys. Res.*, **91**, 11917.

[46] Kirk J. G. 1984 *Proceedings of the Australian Astronomical Society* **5**, 446.

[47] Kirk, J. G. 1988 *Astrophys. J.*, **324**, 557.

[48] Kirk, J. G., Schlickeiser, R. and Schneider, P. 1988 *Astrophys. J.*, **328**, 000.

[49] Kirk, J. G. and Schneider, P. 1987 *Astrophys. J.*, **315**, 425.

[50] Kirk, J. G. and Schneider, P. 1988 submitted to *Astron & Astrophys.*

[51] Kirk, J. G. and Webb, G. M. 1988 *Astrophys. J.* in press.

[52] Königl, A. 1980 *Phys. Fluids* **23**, 1083.

[53] Krymsky, G. F. 1977 *Sov. Phys. Dokl.* **22**, 327.

[54] van der Laan, H. 1966 *Nature* **211**, 1131.

[55] Lagage, P. O. and Cesarsky, C. J. 1981, in *Proceedings of the International School and Workshop on Plasma Astrophysics*, Varenna, ESA SP–161, page 317.

[56] Landau, L. D. and Lifshitz, E. M. 1959 *Fluid Mechanics* (London: Pergamon Press).

[57] Lee, M. A. 1982 *J. Geophys. Res.*, **87**, 5063.

[58] Lee, M. A. 1983 *J. Geophys. Res.*, **88**, 6109.

[59] Lind, K. R. and Blandford, R. D. 1985 *Astrophys. J.*, **295**, 358.

[60] Lindquist, R. W. 1966 *Ann. Phys. (USA)* **37**, 487.

[61] Luhmann, J. G. 1976 *J. Geophys. Res.*, **81**, 2089.

[62] Lyubarskyi, Yu. E. and Sunyaev, R. A. 1982 *Sov. Astron. Lett.* **8**, 330.

[63] Marscher, A. P. 1980 *Astrophys. J.*, **235**, 386.

[64] Marscher, A. P. and Broderick, J. J. 1982 *Astrophys. J.*, **247**, L49.

[65] Marscher, A. P. and Gear, W. K. 1985 *Astrophys. J.*, **298**, 114.

[66] Matthews, J. and Walker, R. L. 1970 *Mathematical Methods of Physics* (Menlo Park, California: Benjamin/Cummings Publishing Co.)

[67] Melrose, D. B. 1969 *Astrophys. and Space Sci.*, **4**, 143.

[68] Melrose, D. B. 1980 *Plasma Astrophysics*, Vol I, (New York: Gordon & Breach).

[69] Melrose, D. B. 1980 *Plasma Astrophysics*, Vol II, (New York: Gordon & Breach).

[70] Mihalas, D. and Mihalas, B. R. 1984 *Radiation Hydrodynamics* (Oxford: Oxford University Press).

[71] Milne, E. A. 1930 *Thermodynamics of the Stars* in *Handbuch der Astrophysik*, **3**, 65, also in *Selected Papers on the Transfer of Radiation*, ed. D. H. Menzel 1966 (New York: Dover).

[72] Pacholczyk, A. G. 1970 *Radio Astrophysics* (San Francisco: Freeman).

[73] Padrielli, L., Fanti, R., Ficarra, A., Gregorini, L., and Mantovani, F. 1986, in *Quasars* IAU Symposium No. 119, eds G. Swarup, V. K. Kapahi (Dordrecht: Reidel), page 149.

[74] Parker, E. N. 1965 *Planet Space Science* **109**, 1328.

[75] Parker, E. N. 1976, in *The Physics of Nonthermal Radio Sources* ed. G. Setti (Dordrecht: Reidel), page 137.

[76] Pauliny-Toth, I. I. K. 1987, in *Superluminal Radio Sources* eds. J. A. Zensus, T. J. Pearson (Cambridge: Cambridge University Press), page 55.

[77] Pauliny-Toth, I. I. K. and Kellermann, K. I. 1966 *Astrophys. J.*, **146**, 634.

[78] Peacock, J. A. 1981 *Mon. Not. R. Astr. Soc.*, **196**, 135.

[79] Pearson, T. J., Unwin, S. C., Cohen, M. H., Linfield, R. P., Readhead, A. C. S., Seielstad, G. A., Simon, R. S. and Walker, R. C. 1981 *Nature* **290**, 365.

[80] Pomraning, G. C. 1973 *The Equations of Radiation Hydrodynamics* (London: Pergamon Press).

[81] Press, W. H., Flannery, B. P., Teukolsky, S. A. and Vetterling, W. T. 1986 *Numerical Recipes* (Cambridge: Cambridge University Press).

[82] Quest, K. B. 1987 *Theory and Simulation of Collisionless Parallel Shocks* submitted to *J. Geophys. Res.*

[83] Rees, M. J. 1967 *Mon. Not. R. Astr. Soc.*, **135**, 341.

[84] Richardson, R. G. D. 1918 *Am. J. Math.*, **40**, 283.

[85] Rickett, B. J. 1986 *Astrophys. J.*, **307**, 564.

[86] Riffert, H. 1986 *Astrophys. J.*, **310**, 729.

[87] Robson, E. I., Gear, W. K., Clegg, P. E., Ade, P. A. R., Smith, M. G., Griffin, M. J., Nolt, I. G., Radostitz, J. V. and Howard, R. J. 1983 *Nature* **305**, 194.

[88] Rossi, B. and Olbert, S. 1970 *Introduction to the Physics of Space* (New York: McGraw-Hill).

[89] Scheuer, P. A. 1984 *Adv. Sp. Res.* **4**, 337 (nos. 2–3).

[90] Scheuer, P. A. G. and Readhead, A. C. S. 1979 *Nature* **277**, 182.

[91] Schlickeiser, R. 1987 submitted to *Ap. J.*

[92] Schneider, P. and Kirk, J. G. 1987 *Astrophys. J.*, **323**, L87.

[93] Sieber, W. 1982 *Astron. and Astrophys.*, **113**, 311.

[94] Sikora M., Kirk J. G., Begelman M. C. and Schneider P. 1987 *Astrophys. J.*, **320**, L81.

[95] Swarup, G. and Kapahi, V. K. 1986 *Quasars* IAU Symposium No. 119, (Dordrecht: Reidel).

[96] Synge, J. L. 1957 *The Relativistic Gas* (Amsterdam: North-Holland Publishing Co.)

[97] Taub, A. H. 1978 *Ann. Rev. Fluid Mech.* **10**, 301.

[98] Tidman, D. A. and Krall, N. A. 1971 *Shock Waves in Collisionless Plasmas* (New York: John Wiley & Sons).

[99] Tsytovich, V. N. 1960 *Plasma Turbulence* (London: Pergamon Press).

[100] Unwin, S. C., Cohen, M. H., Biretta, J. A., Pearson, T. J.,Seielstad, G. A., Walker, R. C., Simon, R. S. and Linfield, R. P. 1985 *Astrophys. J.*, **289**, 109.

[101] Völk, H. J. 1973 *Astrophys. and Space Sci.*, **25**, 471.

[102] Völk, H. J., Morfill, G., Alpers, W. and Lee, M. A. 1974 *Astrophys. and Space Sci.*, **26**, 403.

[103] Webb, G. M. 1985 *Proceedings of the 19th International Cosmic Ray Conference*, La Jolla, **3**, 107.

[104] Webb, G. M. 1987 *Astrophys. J.*, **319**, 215.

[105] Wiener, N. and Hopf, E. 1931 *Berlin. Ber. Math. Phys.* **K1**, 969.

[106] Wilkinson, J. H. 1965 *The Algebraic Eigenvalue Problem* (Oxford: Clarendon Press).

[107] Zachary, A. 1987 *Resonant Alfvén Wave Instabilities Driven by Streaming Fast Particles*, Ph.D. thesis, Lawrence Livermore National Laboratory, University of California.

[108] Zensus, J. A. and Pearson, T. J. 1987 *Superluminal Radio Sources* (Cambridge: Cambridge University Press).